AMERICAN SOCIETY FOR MICROBIOLOGY | Journal of Virology®

VIRUS-CELL INTERACTIONS

Acquisition of Furin Cleavage Site and Further SARS-CoV-2 Evolution Change the Mechanisms of Viral Entry, Infection Spread, and Cell Signaling

Elena I. Frolova,[a] Oksana Palchevska,[a] Tetyana Lukash,[a] Francisco Dominguez,[a] William Britt,[a,b] Ilya Frolov[a]

[a]Department of Microbiology, University of Alabama at Birmingham, Birmingham, Alabama, USA
[b]Department of Pediatrics and Neurobiology, UAB School of Medicine, Birmingham, Alabama, USA

ABSTRACT Circulation of severe acute respiratory syndrome coronavirus 2 (SARS-CoV-2) in the human population leads to further viral evolution. The new variants that arise during this evolution are more infectious. Our data suggest that newer variants have shifted from utilizing both cathepsin/endosome- and TMPRSS2-mediated entry mechanisms to rely on a TMPRSS2-dependent entry pathway. Accordingly, only the early lineages of SARS-CoV-2 are capable of infecting and forming syncytia in Vero/ACE2 cells which lack TMPRSS2 expression. The presence of an intact multibasic furin cleavage site (FCS) in the S protein was a key requirement for cell-to-cell fusion. Deletion of FCS makes SARS-CoV-2 more infectious *in vitro* but renders it incapable of syncytium formation. Cell-to-cell fusion likely represents an alternative means of virus spread and is resistant to the presence of high levels of neutralizing monoclonal antibodies (MAbs) and immune sera in the media. In this study, we also noted that cells infected with SARS-CoV-2 with an intact FCS or alphavirus replicon expressing S protein (VEErep/S) released high levels of free S1 subunit. The released S1 is capable of activating the TLR4 receptor and inducing a pro-inflammatory response. Thus, S1 activation of TLR4 may be an important contributor to SARS-CoV-2-induced COVID-19 disease and needs to be considered in the design of COVID mRNA vaccines. Lastly, a VEErep/S-replicon was shown to produce large amounts of infectious, syncytium-forming pseudoviruses and thus could represent alternative experimental system for screening inhibitors of virus entry and syncytium formation.

IMPORTANCE The results of this study demonstrate that the late lineages of SARS-CoV-2 evolved to more efficient use of the TMPRSS2-mediated entry pathway and gradually lost an ability to employ the cathepsins/endosome-mediated entry. The acquisition of a furin cleavage site (FCS) by SARS-CoV-2-specific S protein made the virus a potent producer of syncytia. Their formation is also determined by expression of ACE2 and TMPRSS2 and is resistant to neutralizing human MAbs and immune sera. Syncytium formation appears to be an alternative means of infection spread following the development of an adaptive immune response. Cells infected with SARS-CoV-2 with an intact FCS secrete high levels of the S1 subunit. The released S1 demonstrates an ability to activate the TLR4 receptor and induce pro-inflammatory cytokines, which represent a hallmark of SARS-CoV-2 pathogenesis. Alphavirus replicons encoding SARS-CoV-2 S protein cause spreading, syncytium-forming infection, and they can be applied as an experimental tool for studying the mechanism of syncytium formation.

KEYWORDS ACE2, S1 secretion, SARS-CoV-2, TLR4, TMPRSS2, furin cleavage, pseudoinfectious viruses, spike protein, syncytium, viral evolution

The recently emerged severe acute respiratory syndrome coronavirus 2 (SARS-CoV-2) has demonstrated an unprecedented spread throughout the world. It has also demonstrated rapid evolution, and new variants of SARS-CoV-2 with higher transmission

Editor Tom Gallagher, Loyola University Chicago

Address correspondence to Ilya Frolov, ivfrolov@uab.edu.

The authors declare no conflict of interest.

Received 10 May 2022
Accepted 1 July 2022
Published 25 July 2022

rates (1–5) continue to appear in circulation every few months. The associated COVID-19 has already caused a health crisis and millions of deaths worldwide (6, 7). To date, approved therapeutic interventions and vaccination remain limited and, to date, have failed to prevent the spread of infection.

SARS-CoV-2 is a member of the *Betacoronavirus* genus (β-CoV) in the *Coronaviridae* family (8). This is a spherical virus containing a lipid envelope with embedded glycoprotein spikes. The SARS-CoV-2 genome (G RNA) is represented by a positive-sense, single-stranded RNA of ~30 kb in length, the largest among all of the RNA genome-containing viruses (9). G RNA mimics cellular mRNA in that it has a cap and a poly(A)-tail at the 5′ and 3′ termini, respectively. In infected cells, this RNA is directly translated into two long overlapping polyproteins (ORF1a and ORF1ab). These are further processed into individual nonstructural proteins (nsp1-to-16) by proteases encoded by the virus and function in replication of the viral genome, synthesis of 8 subgenomic RNAs (SG RNAs), and modification of the intracellular environment to promote viral replication (10). SG RNAs encode additional accessory proteins, whose functions are only partially understood, and structural proteins, which form SARS-CoV-2 virions (11). The functions of the structural N protein include packaging of viral G RNA into helical nucleocapsid (NC) during formation of infectious viral particles. It also stimulates the synthesis of virus-specific RNAs, but the mechanism of this function remains obscure (11). The structural M and E proteins contribute to virion assembly and are embedded in the viral lipid envelope. Both M and E are required for virus release and its infectivity. Another structural protein, the spike (S) protein, forms trimeric spikes on the surface of virions and is a major determinant of viral infectivity, spread, pathogenesis, and adaptation for infection of new hosts and cell lines (9). In the early steps of viral infection, it mediates binding of the virions to the ACE2 receptor and additional attachment factors such as glycosaminoglycans (GAGs), including heparan sulfate (HS) (12). The S protein also functions in the fusion between the viral lipid envelope and cellular membranes, leading to NC release into the cytoplasm (13, 14). Accumulating data also suggest that the S protein in SARS-CoV-2 can use additional proteins at the plasma membrane as alternative receptors or utilizes ACE2 from other species for entry into cells (15–18). To date, SARS-CoV-2 has demonstrated a capacity to replicate in a broad range of mammalian cell lines, including multiple human, primate, mouse, and hamster cell lines, if cells from these different species are engineered to express human ACE2 receptor (12). These data provide a strong argument for receptor-mediated entry being the primary barrier against infection spread to multiple tissues and species.

After attaching to cells, SARS-CoV-2 utilizes at least two entry mechanisms. In the first entry pathway, in the cells expressing the transmembrane serine protease TMPRSS2. The later protease mediates cleavage of the S2′ site to release the fusion peptide that ultimately facilitates fusion of the viral lipid envelope and plasma membrane. In cells lacking TMPRSS2 protease, the S2′ processing is achieved by cathepsins, and fusion of viral envelope takes place in the endosomes (14, 19).

SARS-CoV-2 shares most of its structural characteristics and replication program with SARS-CoV, which was responsible for a severe disease outbreak in the early 2000s. A striking difference between the SARS-CoV and SARS-CoV-2 is that the S protein of SARS-CoV-2 contains an additional stretch of basic amino acids which serves as a furin cleavage site (FCS) (20). However, it should be noted that other cellular proteases can also be involved in its processing (21). FCS mediates processing of the S protein into S1/S2 subunits before or during the release of infectious particles from infected cells (22). This multibasic peptide is present in all SARS-CoV-2 isolates from humans and is functional as evidenced by the finding that released virions contain both uncleaved S protein and readily detectable levels of S1 and S2. Interestingly, processing of the S protein into S1 and S2 appears to be disadvantageous for propagation of SARS-CoV-2 *in vitro* in many ACE2-expressing cell lines. Virus isolates from humans rapidly evolve *in vitro* and accumulate deletions or mutations in the FCS, which either have strong negative effects on the efficiency of S protein processing or completely abrogate it (12, 23, 24). Viral mutants that arise *in vitro* demonstrate higher infectivity for cultured cells but are detectably less pathogenic in small animal models (25). Thus, the presence of FCS in the S

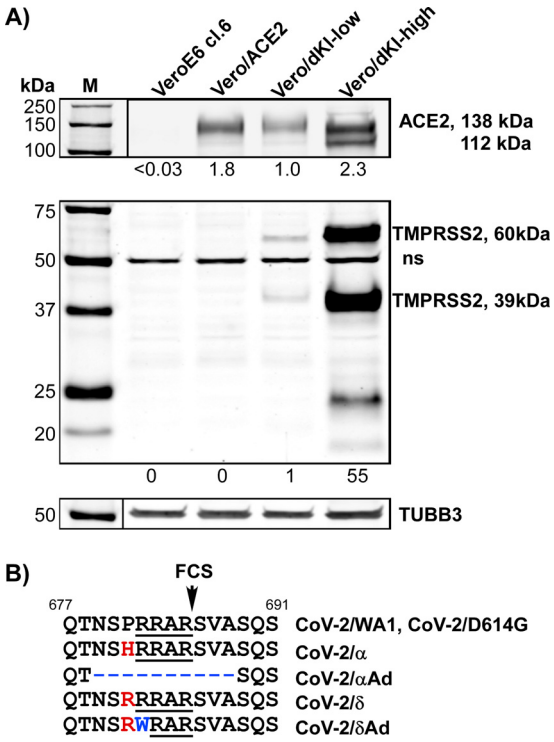

FIG 1 Cell lines and SARS-CoV-2 variants used in the study. (A) The levels of hACE2 and hTMPRSS2 expression in Vero cells and their KI derivatives were determined by Western blotting (WB) using antibodies against ACE2 and corresponding secondary fluorescent antibodies. Membranes were scanned on a LI-COR imager. Relative levels of proteins were determined using Empiria Studio software (LI-COR) and normalized to the levels of tubulin-β3. "ns" indicates a nonspecific band. (B) Amino acid sequences of the S protein fragments containing furin cleavage site (FCS). The FCS sequences are underlined. Mutations are indicated in red and blue, and the deletion is shown by dashes. Arrow indicates the position of cleavage in the wild-type S protein.

protein appears to make viral replication and spread more efficient *in vivo*, while it becomes disadvantageous for *in vitro* virus propagation in cells expressing no or low levels of TMPRSS2.

In this new study, we further investigated SARS-CoV-2 evolution and the role of the furin-mediated processing of the S protein in viral infection. Our data demonstrate that while circulating in the human population, SARS-CoV-2 evolves to use the TMPRSS2-mediated entry pathway more efficiently and loses the ability to utilize cathepsins/endosome-mediated entry. In addition, cells producing S protein with an intact FCS from alphavirus replicon efficiently form syncytia and release pseudoviruses that readily spread *in vitro*. Syncytium formation is determined by the presence of ACE2 and high levels of TMPRSS2 expression. This cell-to-cell fusion is also highly resistant to human neutralizing monoclonal antibodies (hMAbs) and sera of immunized individuals. Lastly, cells infected with SARS-CoV-2 release not only virions but also high levels of the S1 subunit into the medium. S1 subunit release does not depend on SARS-CoV-2 replication, as the expression of the S protein from alphavirus replicons also results in efficient secretion of the S1 protein. The secreted S1 can activate the TLR4 receptor and induce pro-inflammatory cytokines, which represent a hallmark of SARS-CoV-2 pathogenesis.

RESULTS

Generation of cell lines and recovery of SARS-CoV-2 from human specimens. In this study, we used a variety of Vero cell derivatives. The parental Vero E6 cell line was obtained from ATCC. Vero/ACE2 cells were designed to express high levels of ACE2. As Vero E6, they expressed levels of TMPRSS2 that were undetectable by either Western blot (WB) (Fig. 1A) or PCR (data not shown). The double knock-in Vero/dKI-high cell line

stably expressed high levels of both ACE2 and TMPRSS2, and in Vero/dKI-low cells, the expression of human TMPRSS2 was about 50-fold lower than in Vero/dKI-high cell line (Fig. 1A). In Vero/dKI-high cells, we also observed efficient cleavage of ACE2 (Fig. 1A).

We used a number of natural isolates of SARS-CoV-2. The original CoV-2/WA1 variant was recovered on Vero E6 cells and, after 4 or 5 passages on the same cells, was distributed by the CDC to numerous research laboratories. The second variant CoV-2/D614G (26) was recovered on Vero/ACE2 cells (12). Based on sequencing data, both CoV-2/WA1 and CoV-2/D614G retained intact FCS for at least two passages in Vero/ACE2 cells. Within a few hours postinfection (p.i.), Vero/ACE2 cells infected with either virus formed syncytia and small plaques developed on both Vero E6 and Vero/ACE2 (12).

The Alpha and Delta variants of SARS-CoV-2 (termed here CoV-2/α and CoV-2/δ, respectively) obtained from nasopharyngeal swabs from infected humans exhibited different characteristics. The initial attempts to recover them by infecting Vero E6 and Vero/ACE2 cells with multiple swab samples were unsuccessful. Although cells infected with some samples ultimately developed a cytopathic effect (CPE), the viruses recovered from these cultures had their FCSs either mutated or deleted (Fig. 1B). Two cell culture-adapted variants, termed CoV-2/αAd and CoV-2/δAd, were chosen for use in some experiments presented in the following sections. However, most samples produced no CPE, and viral release was not detected by either plaque assay or immunostaining (data not shown). This indicated that, in contrast to earlier circulating variants, expression of only the ACE2 protein was insufficient for infection of cells and virus spread. Indeed, the double knock-in (dKI) cell lines, which also expressed TMPRSS2 besides ACE2, Vero/dKI-low, and Vero/dKI-high in particular, were found to be highly efficient for the recovery of CoV-2/α and CoV-2/δ. Upon infection with the swab materials, which produced no spreading infection in Vero/ACE2 cells, the dKI cells supported virus replication and spread, rapidly developing syncytia and CPE. Both CoV-2/α and CoV-2/δ produced large plaques on Vero/dKI-high and Vero/dKI-low cells, and based on microscopic observation, these plaques were the result of the development and ultimate destruction of large syncytia formed under an agarose overlay. Sequencing of the S gene in the recovered variants after two passages in Vero/dKI cells did not detect mutations in their FCSs (Fig. 1B).

SARS-CoV-2 isolates infect ACE2 and TMPRSS2 KI derivatives of Vero cells with different efficiencies. To further understand the differences between natural isolates, we compared the infectivity of the prototype CoV-2/WA1, CoV-2/D614G, CoV-2/α, and CoV-2/δ, and the cell culture-adapted variants in Vero/ACE2 and Vero/dKI-high cell lines. Vero/ACE2 cells were utilized to support infection by viruses capable of using the endosome-mediated entry pathway (but not the TMPRSS2-dependent pathway), which requires functional endosomal cathepsins for S2/S′ processing. Vero/dKI-high cells can support virus entry via both the endosome pathway and the TMPRSS2-dependent S protein processing pathway. The latter pathway results in direct fusion of viral and plasma membranes. The infectious titers of the virus samples were determined on both cell lines and compared to the concentrations of viral RNA in the released virions, determined by quantitative reverse transcription PCR (RT-qPCR) as genome equivalents per mL (GE/mL). The data presented in Fig. 2A and B demonstrate that the early variants, CoV-2/WA1 and CoV-2/D614G, were able to efficiently utilize the TMPRSS2-independent, endosome-mediated entry pathway in Vero/ACE2 cells. The CoV-2/α variant was less efficient in endosome-mediated entry into Vero/ACE2 cells (Fig. 2A and B). The CoV-2/δ variant appeared completely dependent on the TMPRSS2-dependent pathway and could not use the endosomal entry route in our experimental system. The ratio of GE/mL to PFU/mL in Vero/ACE2 cells increased from $\sim$200 for CoV-2/WA1 to more than 2×10^6 for CoV-2/δ. Notably, this ratio could not be accurately quantitated for CoV-2/δ, because on Vero/ACE2 cells, this variant was unable to produce plaques or cause CPE. Therefore, we estimated titers of 50 PFU/mL (equivalent to the limit of detection) for our calculations.

The ACE2/TMPRSS2-dependent entry directly through the plasma membrane was more efficient for all variants studied because the titers determined on Vero/dKI-high

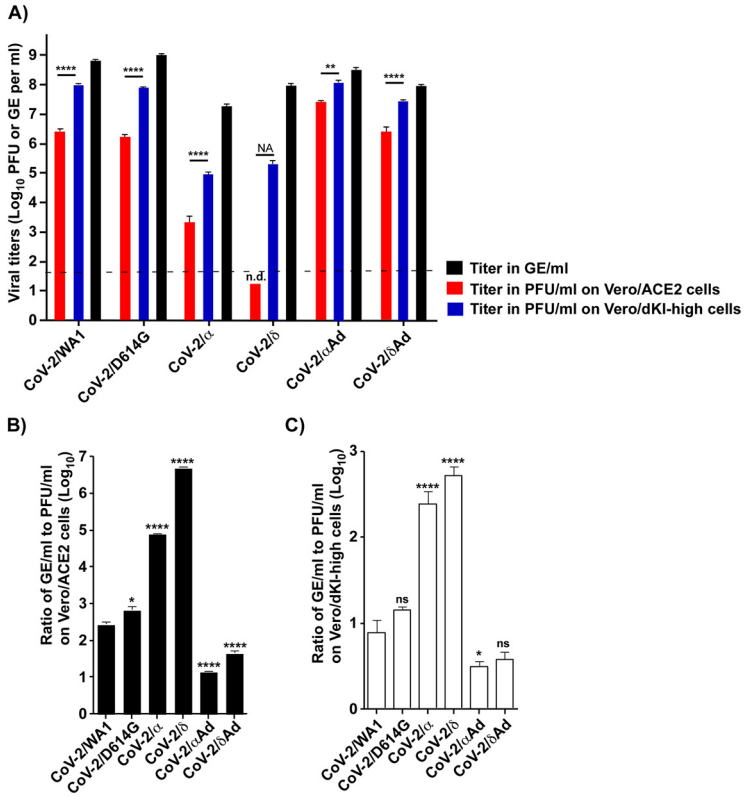

FIG 2 Four lineages of SARS-CoV-2 infect Vero cell derivatives with different efficiencies. (A) Viral samples were simultaneously titrated by plaque assay on Vero/ACE2 and Vero/dKI-high cells and used in RT-qPCR to determine viral concentrations in genome equivalents per mL (GE/mL). Means and standard deviations (SDs) are presented. Dashed line shows the limit of viral detection in plaque assay. "n.d." indicates that plaques were not detectable. (B and C) Ratios of viral particle concentrations in the samples, determined in GE/mL, to viral infectious titers, determined in PFU/mL on Vero/ACE2 and Vero/dKI-high cell lines. Significant differences, as shown in panels (A, B, and C) were determined by one-way analysis of variance (ANOVA) Dunnett's test (*, $P < 0.05$; **, $P < 0.01$; ***, $P < 0.001$; ****, $P < 0.0001$; $n = 3$). "NA" indicates that statistical analysis is not applicable.

cells were always higher than those on the Vero/ACE2 counterpart (Fig. 2A). However, its role was particularly evident in the case of CoV-2/δ infection. Interestingly, for Vero/dKI-high cells, the GE/PFU ratios of CoV-2/α and CoV-2/δ samples remained higher than those of CoV-2/WA1 and CoV-2/D614G (Fig. 2A and C). Thus, there is a possibility that in other cells, CoV-2/α and CoV-2/δ utilize additional host proteins in the cell entry process, which are not present in Vero E6 and its KI derivatives.

In the same set of experiments, we also analyzed the viruses which adapted to efficiently replicate in Vero/ACE2 cells (Fig. 2A to C). CoV-2/δAd encoded a mutated FCS, and CoV-2/αAd had the entire multibasic FCS deleted (Fig. 1B). Both the deletion of FCS and the acquired mutation, which strongly affected S1/S2 processing, appeared to restore the ability of the viruses to enter the cells via the endocytic route. Thus, they became capable of efficient infection of Vero/ACE2 cells expressing no TMPRSS2 and their GE:PFU ratios, assessed on Vero/ACE2 cells, decreased by a few orders of magnitude (Fig. 2A and B). Accordingly, the growth rates and infectious titers of the CoV-2/δAd and CoV-2/αAd mutants on Vero/dKI cells were dramatically higher than those of the parental, non-cell culture-adapted viruses (Fig. 3).

All of the initial virus isolates efficiently formed syncytia in Vero/dKI-high cells (Fig. 4). However, the deletion of the entire FCS in the cell culture-adapted CoV-2/αAd made the virus completely incapable of inducing cell-to-cell fusion. On the other hand, partial inactivation of furin-mediated processing by point mutations in cell culture-adapted CoV-2/δAd

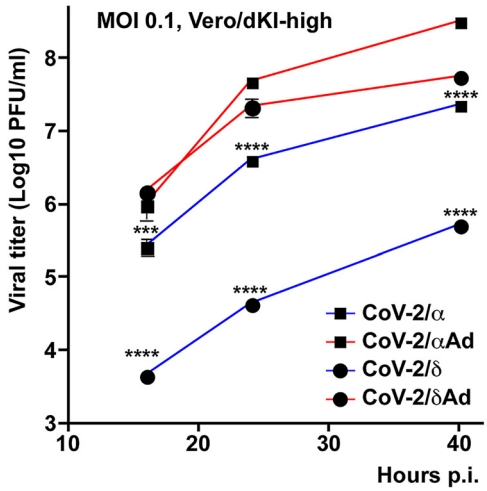

FIG 3 Cell culture-adapted variants of SARS-CoV-2 with mutated FCS replicate more efficiently and to higher titers in Vero/dKI-high cells. Vero/dKI-high cells in 6-well Costar plates were infected with the indicated cell culture-adapted viruses and the corresponding parental isolates at a multiplicity of infection (MOI) of 0.1 PFU/cell. At the indicated times postinfection (p.i.), media were replaced, and viral titers were determined by plaque assay on Vero/dKI-high cells. Significance of differences was determined by two-way ANOVA Tukey's tests (***, $P < 0.001$; ****, $P < 0.0001$; $n = 3$).

(Fig. 1B) and in the previously designed recombinant CoV-2/GFP/S686G variant (12) did not abrogate their capacity to induce fusion of dKI cells. These variants continued to form syncytia in the Vero/dKI-high cell line, but not in Vero/ACE2 cells (data not shown).

FCS processing and syncytium formation are beneficial for virus spread. One of possible benefits of acquiring FCS and syncytium formation for SARS-CoV-2 biology could be to use this additional mechanism for cell-to-cell virus spread in the presence of antiviral adaptive immune responses. Therefore, we next investigated whether this mechanism of viral spread is resistant to SARS-CoV-2 specific neutralizing antibodies (Abs). The main analyses were performed using receptor-binding domain (RBD)-specific neutralizing human

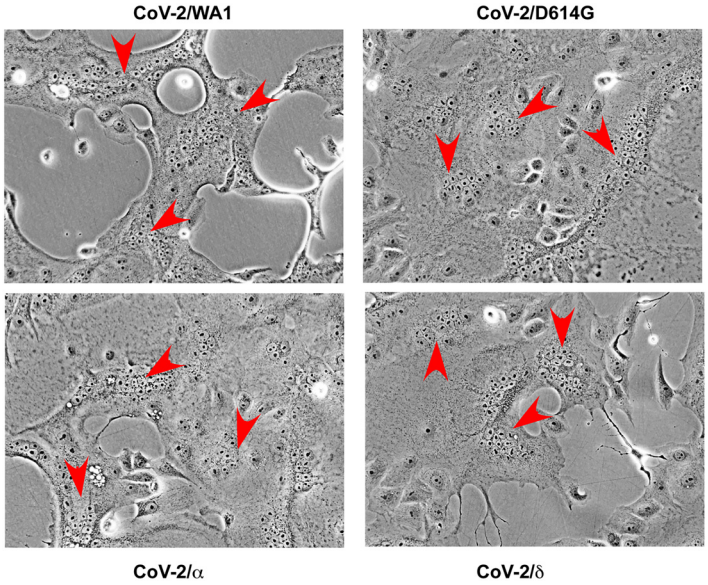

FIG 4 All SARS-CoV-2 isolates with intact FCS efficiently formed syncytia in Vero/dKI-cells. Cells were seeded into 6-well Costar plates and infected with the indicated viruses at an MOI of 0.01 PFU/cell. Images were acquired at 18 hours p.i. on an EVOS inverted microscope. Syncytia are indicated by red arrowheads.

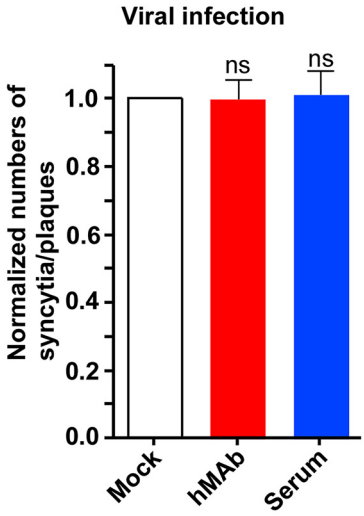

FIG 5 Highly potent human neutralizing monoclonal antibody (MAb) and immune serum do not affect syncytium formation by CoV-2/α. Vero/dKI-high cells in 6-well Costar plates were infected with ~100 PFU of CoV-2/α. They were then incubated in Dulbecco's modified Eagle medium (DMEM) supplemented with 3% fetal bovine serum (FBS) and containing either hMAbs 1213H7 or immune serum 7,000 at concentrations of 4 μg/mL and 1:100 dilution, respectively. At 2 days p.i., cells were fixed with 4% paraformaldehyde (PFA) and stained for plaques with crystal violet. The control mock-treated, virus-infected cells were covered by agarose as in the plaque assay (see Materials and Methods). Data were normalized to the number of plaques formed in mock-treated, infected cells under agarose cover. Means and SDs are presented. Significance of differences was determined by one-way ANOVA Dunnett's test (ns, $P > 0.05$; $n = 3$).

monoclonal antibody (hMAb) 1213H7 (27, 28) and two human immune sera. Samples were tested with replication-competent CoV-2/α in a standard plaque reduction neutralization test (PRNT; see Materials and Methods for details). The 50% inhibitory concentration (IC_{50}) of the used hMAb was <20 ng/mL and the 50% plaque reduction neutralization titers ($PRNT_{50}$) for the sera were 7,000 and 4,000 (these were designated serum 7,000 and serum 4,000, respectively). To study the effects of Abs on syncytium formation, Vero dKI-high cells were infected with ~100 PFU of CoV-2/α and then incubated in media supplemented with hMAb or serum at different dilutions (see Fig. 5 and Materials and Methods for details). By 48 hours p.i., the infected, mock-treated cell monolayers demonstrated complete CPE due to virus spread. Regardless of their concentrations in the media, hMAb and both immune sera (Fig. 5 and data not shown) failed to stop syncytium development, but prevented virus spread by infection of new cells. The numbers of syncytia formed were equal to the number of plaques in the infected, mock-treated cells incubated under agarose overlays. Agarose overlays were used to prevent spread of the infection beyond the syncytia which formed by primarily infected cells. Figure 5 presents the results of a representative experiment performed with the highest concentration of hMAb (4 μg/mL) and immune serum 7,000 (1:100 dilution). Thus, S protein-specific neutralizing hMAbs and high titer sera added after the initial infection had no detectable impact on syncytium formation in Vero/dKI-high cells.

To confirm these data, we used another experimental system. The entire S gene of CoV-2/WA1 variant was cloned under the control of the subgenomic promoter into a replicon of Venezuelan equine encephalitis virus (VEEV) (VEErep/S) (Fig. 6A). The *in vitro*-synthesized replicon and helper RNAs were co-electroporated into cells (see Materials and Methods for details). The titers of harvested S protein-encoding replicons packaged into the VEEV envelope approached 4 to 10 $\times$ 10^8 infectious units (inf.u)/mL, and these particles were used to infect Vero-based cell lines using a low multiplicity of infection (MOI) (Fig. 6B). As for SARS-CoV-2, the fusogenic activity of the S protein expressed by VEErep/S were strictly dependent on the presence of ACE2 protein at the plasma membrane. Vero E6 cells with levels of ACE2 that were undetectable by WB did not support syncytium formation, but Vero/ACE2 cells did (Fig. 6C). Expression of TMPRSS2 in two independent Vero/dKI cell

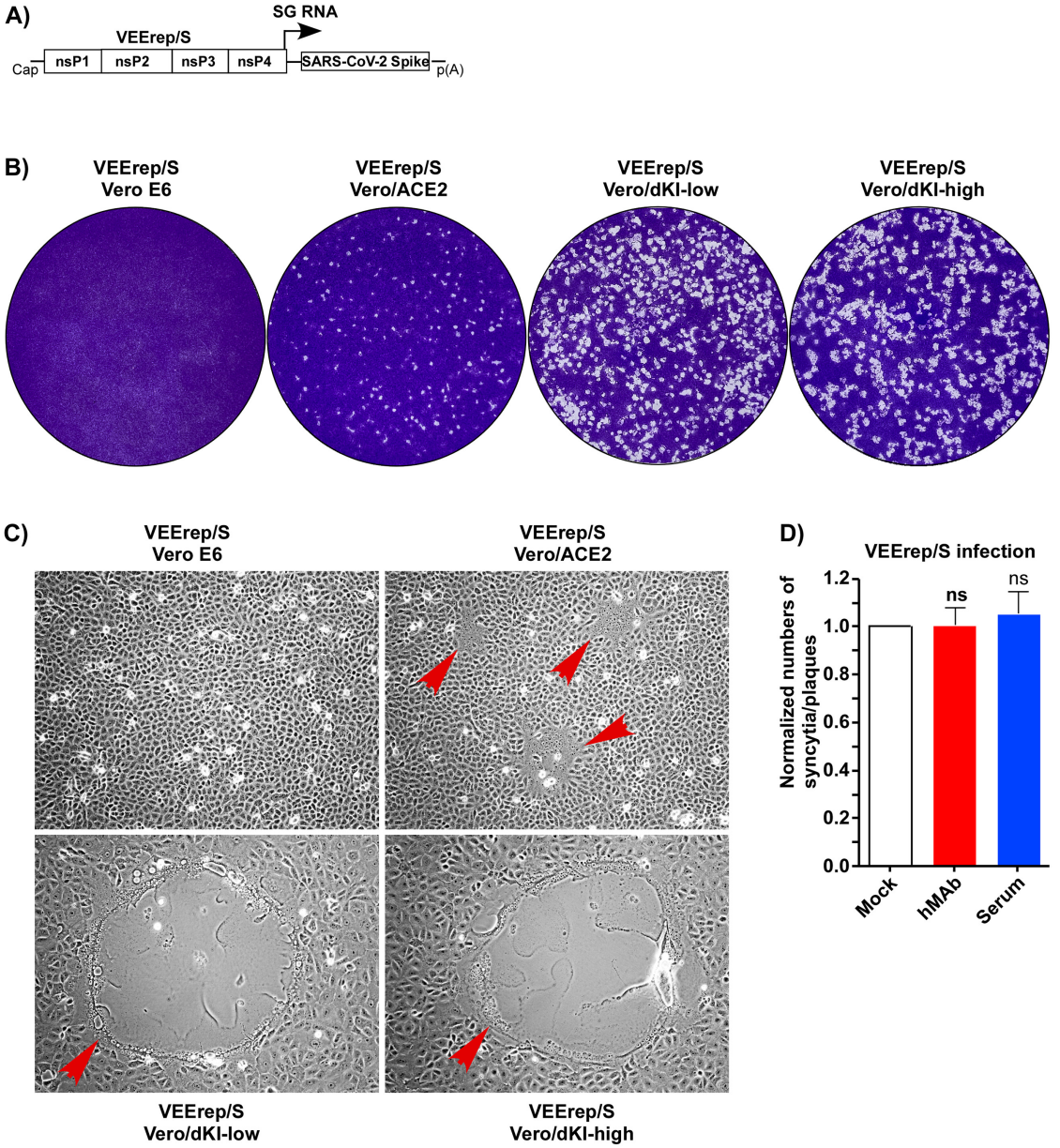

FIG 6 Upon infection with packaged VEErep/S replicon, Vero cells expressing ACE2 or ACE2 and TMPRSS2 form syncytia, which are resistant to SARS-neutralizing Abs. (A) Schematic of the VEErep/S replicon. (B) Indicated cell lines were seeded into 6-well Costar plates and infected with packaged VEErep/S replicon. Cells were then incubated for 18 h in complete medium, fixed with PFA, and stained with crystal violet. (C) Before staining, images of standard-size syncytia were acquired on a Nikon Eclipse inverted microscope. Syncytia are indicated by red arrows. This experiment was repeated multiple times, and syncytia were reproducibly of the same sizes. (D) Vero/dKI-high cells in 6-well Costar plates were infected with ~100 infectious units (inf.u) of packaged VEErep/S. They were then incubated in DMEM supplemented with 3% FBS and containing either hMAbs 1213H7 or immune serum 7,000 at concentrations of 4 μg/mL and 1:100 dilution, respectively. At 18 hours p.i., cells were fixed with 4% PFA and stained for plaques with crystal violet. Data were normalized to the numbers of plaques in mock-treated cells. Means and SDs are presented. Significance of differences was determined by one-way ANOVA Dunnett's test (ns, $P > 0.05$; $n = 3$).

lines (Vero/dKI-high and Vero/dKI-low) had a strong positive effect on syncytium size. In Vero/ACE2 cells, each formed syncytium contained 5-to-20 nuclei, and in Vero/dKI-low and Vero/dKI-high cells, they contained between 100 and 150 nuclei of the fused cells (Fig. 6C). Thus, as in the case of SARS-CoV-2 infection, efficient syncytium formation was dependent on expression of both ACE2 and TMPRSS2 proteins.

Next, we used these packaged VEErep/S replicons to infect Vero/dKI-high cells at a dose of ~100 inf.u/well and further incubated them in the presence of the highest achievable concentrations of hMAb 1213H7 and immune serum 7,000 (4 μg/mL and

1:100 dilution, respectively). Within 18 to 20 hours p.i., large syncytia were formed around the primarily infected cells (Fig. 6D). As in the experiments with live virus, there was no noticeable effect of the hMAbs of immune sera on the size of syncytia produced by the VEErep/S replicon.

Interestingly, Vero/dKI-high cells, and the Vero/dKI-low cell line in particular, infected with VEErep/S were found to release infectious pseudoviruses to titers approaching 2.5×10^6 inf.u/mL. These pseudoviruses continued to infect and form syncytia on both Vero/dKI-high and Vero/dKI-low cells, the sizes of which were indistinguishable from those of syncytia formed after infection with the originally packaged VEErep/S replicon. Supernatants harvested from these cultures were capable of infecting naive Vero/dKI cells and were passaged multiple times without a decrease in infectious titers. The formation of similar pseudoviruses was previously described for the Semliki Forest virus-based replicon expressing the G protein of vesicular stomatitis virus (VSV) (29, 30). Thus, the infectious VEErep/S pseudovirions most likely represented small, cell-released vesicles containing S protein on their surface. These vesicles contained either replicon genomes or VEEV-specific replication complexes with double-stranded RNA replication intermediates. Since the exact composition of pseudoviruses was not the focus of our study, their detailed characterization has not been performed. However, we were interested in whether their infectivity was based on the same mechanism(s) as that used by SARS-CoV-2 and thus, whether the infection was sensitive to neutralizing Abs. Alternatively, the infection could be resistant to neutralizing Abs and similar to the S protein-mediated cell-to-cell fusion and syncytium formation exhibited by the S protein-expressing cells. To distinguish between these possibilities, we again used a standard PRNT (see Materials and Methods for details) using hMAb 1213H7. For the VEErep/S pseudovirus, the IC_{50} of the hMAb was 30 ng/mL, which was very close to that identified for SARS-CoV-2 virions. Thus, we concluded that the released pseudoviruses used the same entry/infectivity pathway(s) as the authentic virus for infecting cells, but not a syncytium formation-like mechanism which was resistant to neutralizing Abs.

Taken together, these data suggested that the development of syncytia by SARS-CoV-2 requires the presence of ACE2 and TMPRSS2 at the plasma membrane. However, the mechanism for syncytium formation appeared to be different from that used for virus entry. In agreement with previously published data (31, 32), syncytium formation by replicating SARS-CoV-2 and VEErep/S was resistant to highly efficient RBD-specific neutralizing hMAbs and polyclonal SARS-CoV-2-specific human serum. However, these experiments were limited to a few available samples of hMAb and sera. Some published data also suggest that Abs capable of inhibiting syncytium formation are rare, but can be present in some immune sera (32, 33).

Overexpression of TMPRSS2 causes aberrant processing of the S protein. Next, we used the alphavirus replicon-based S protein-expressing system to determine whether the furin-mediated processing of the S protein is an absolute requirement for syncytium development. Vero/ACE2, Vero/dKI-low, and Vero/dKI-high were infected with packaged VEErep/SΔFCS, which encoded SARS-CoV-2 protein with a deleted FCS (Fig. 7A). No syncytium formation was detected in the Vero/ACE2 or Vero/dKI-low cell lines (Fig. 7B). However, Vero/dKI-high cells did produce syncytia (Fig. 7B), albeit they were smaller than those formed by VEErep/S (Fig. 6B). These data suggested that overexpression of TMPRSS2 in Vero/dKI-high cells could potentially cause S protein processing required for membrane fusion, even without furin-mediated pre-cleavage. Indeed, in Vero/dKI-high cells infected with CoV-2/D614G, the spectrum of S protein-derived polypeptides was different from those in other Vero-based cell lines, expressing either low levels of TMPRSS2 or no TMPRSS2 (Fig. 8). Vero/ACE2 and Vero/dKI-low cells infected with CoV-2/D614G demonstrated accumulation of both full-length S protein and its S2 subunit. In Vero/dKI-high cells, the S2 subunit was present at lower levels than in Vero/dKI-low cells. Moreover, in repeat experiments, we detected the presence of a band reminiscent of S2′, and several additional protein bands of similar size. Interestingly, in the virions released from Vero/dKI-high cells, the level of S2 was also low and additional shorter S2

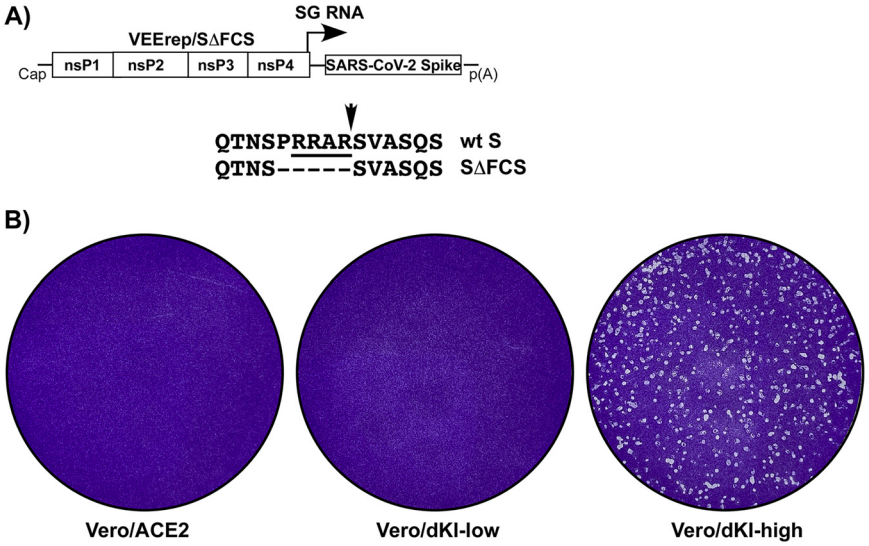

FIG 7 Expression of SARS-CoV-2 S protein that lacks FCS induces syncytium formation only in the ACE2-expressing Vero cells, which also overproduce TMPRSS2. (A) Schematic presentation of the VEErep/SΔFCS replicon and aa sequence of the protein fragment with deleted FCS. (B) Packaged replicon was titrated in parallel in 6-well Costar plates on the indicated cell lines. After incubation for 18 h in liquid media, cells were fixed and stained with crystal violet. Wells infected with the same viral dilution are presented.

derivatives were present (Fig. 8). Since CoV-2/D614G caused rapid syncytium formation and CPE in Vero/dKI-high cells, the aberrant cleavage products of the S protein, as well as N, nsp1, and tubulin, were also detectable in the supernatant after pelleting virions by ultracentrifugation. Thus, high levels of TMPRSS2 expression likely leads not only to cleavage of ACE2 (Fig. 1A), but also to premature processing of S2′ site and/or additional nonspecific cleavage(s) of S2. This observation explains the syncytium formation in Vero/dKI-high by the S protein produced by VEErep/SΔFCS (Fig. 7B). Thus, the interpretation of data describing S protein processing generated in the TMPRSS2-overexpressing cell lines should be done cautiously.

SARS-CoV-2 infection results in secretion of the S1 subunit. During the above-described experiments and other experiments with natural viral isolates, we noticed that after pelleting the viruses produced in cells expressing low levels of TMPRSS2, the supernatants contained high levels of S1, while S2 and S were undetectable. To better understand this effect, we analyzed accumulation of S1 in the harvested media, the pelleted viral particles, and the supernatants from cells infected with different SARS-CoV-2 variants. For infection, we used CoV-2/WA1 and CoV-2/D614G isolates, which retained a functional FCS (Fig. 1A). The tissue culture-adapted CoV-2/δAd and CoV-2/αAd had mutations either strongly affecting or completely eliminating the S protein processing and were used as controls (Fig. 1A). Vero/ACE2 cells were infected with the indicated viruses and further incubated in serum-free media (see Materials and Methods for details). To avoid contamination of samples with intracellular proteins, virus-containing media were harvested at 20 hours p.i., before the cells lost their integrity.

WB analysis demonstrated that the media of CoV-2/WA1- and CoV-2/D614G-infected cells contained both full-size S protein and the S1 and S2 subunits (Fig. 9A). This was expected, as S1/S2 cleavage of portions of the S protein occurs during virus egress. However, the fraction of S1 in the S/S1 bands was repeatedly higher than the fraction of S2 (Fig. 9A). The infected cells also retained more S2 than S1 subunit (Fig. 9A). These data suggested that S1 might be secreted from infected cells and present in the medium not only as a component of viral particles, but also in free form. In agreement with previously published data, only small amounts of S1 or no S1 at all were detected in samples of media harvested from CoV-2/δAd- and CoV-2/αAd-infected cells, respectively.

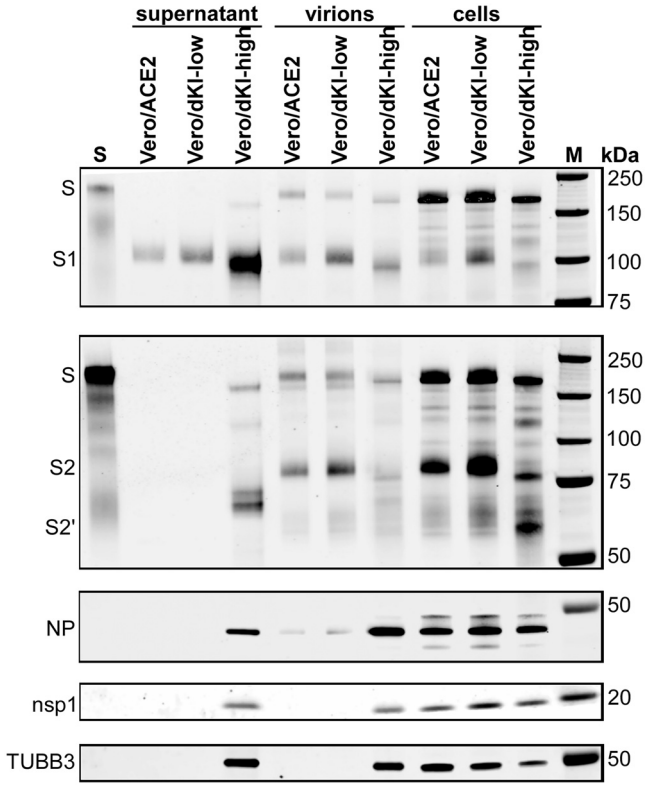

FIG 8 Overexpression of TMPRSS2 leads to aberrant processing of the S protein. The indicated cell lines were infected with CoV-2/D614G at an MOI of 1 PFU/cell. They were incubated in serum-free media for 16 h, and then media and cells were harvested. After UV inactivation, virions were pelleted by ultracentrifugation. Supernatants, pelleted virions, and cell lysates were analyzed by WB as described in Materials and Methods.

Released viruses were inactivated by UV (see Materials and Methods for details), then pelleted by ultracentrifugation, and viral pellets and supernatants were analyzed by WB. Pellets of CoV-2/WA1 and CoV-2/G614G, but not the supernatants, contained the full-length S protein, S1 and S2 subunits, and N protein, reminiscent of being virion components (Fig. 9A). However, only the S1 subunit was clearly detected in the supernatants (Fig. 9A). The lack of N protein in the supernatants after ultracentrifugation confirmed the absence of viral particles and lack of cell lysis, which could lead to nonspecific release of S1. Thus, the S1 subunits in the supernatants were present in free form, but not as virion components. Low levels of S1 were also detectable in the supernatants of cells infected with CoV-2/δAd, which demonstrated some S1/S2 processing.

In additional experiments, we evaluated whether the secretion of the S1 subunit is specific to the earlier circulated SARS-CoV-2 variants or a common phenomenon for all of them. Vero/dKI-low cells were infected with CoV-2/WA1, CoV-2/G614G, CoV-2/α, and CoV-2/δ. As above, media, supernatants and pellets were analyzed for the presence of S, S1, and S2 proteins. Replication of all these viruses resulted in the release of free S1 into the media (Fig. 9B). Notably, CoV-2/δ demonstrated the highest S1 secretion, most likely due to the presence of an additional Arg in FCS, and its viral particles contained the lowest levels of unprocessed S protein. Taken together, these data strongly suggested that infection with any of the tested SARS-CoV-2 variants results in release of the S1 subunit from infected cells not only within virions but also in a free form. Thus, S1 could potentially have additional function(s) in either viral replication or pathogenesis.

Viral replication is not a prerequisite of S1 secretion. In the following experiments, we analyzed whether viral replication is required for secretion of the S1 protein. The above-described VEErep/S replicon (Fig. 6A), which was packaged into infectious

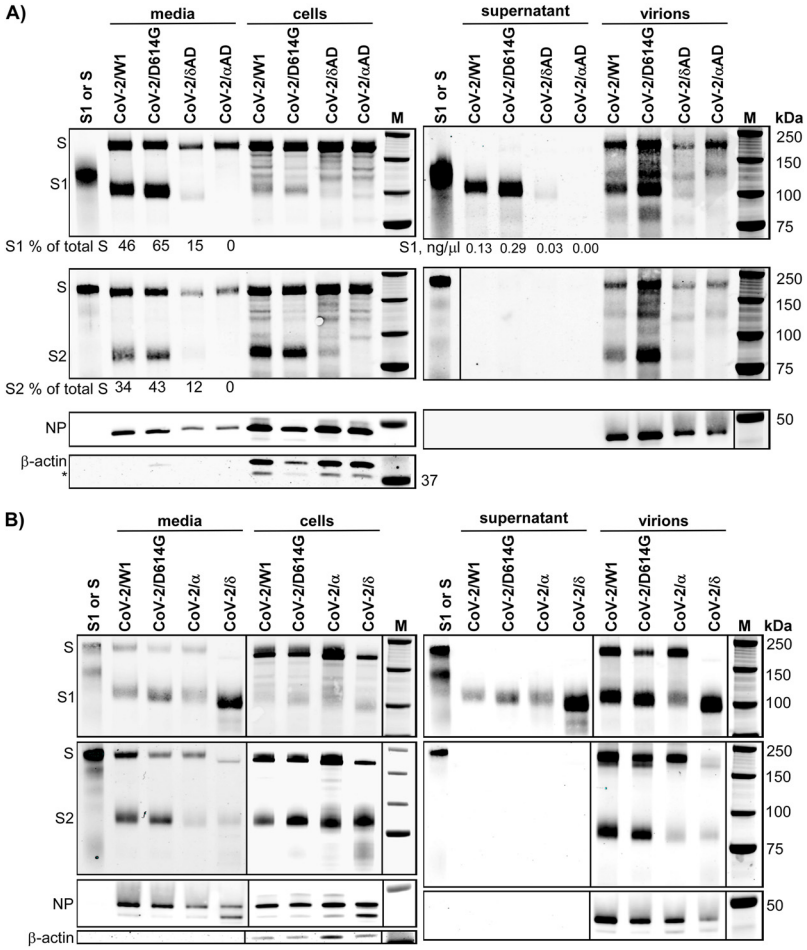

FIG 9 Replication of SARS-CoV-2 variants with intact FCS results in secretion of the S1 subunit. (A) Vero/ACE2 cells were infected with the indicated viruses having either intact or mutated FCS. After incubation of infected cells in serum-free medium for 18 h, the presence of S, S1, S2, and N was analyzed in the cell lysates, medium, and supernatants and pellets after UV inactivation and ultracentrifugation. (B) Vero/dKI-low cells were infected with indicated viruses at an MOI of 1 PFU/cell. After incubation in serum-free medium, the presence of S, S1, S2, and N was analyzed in the cell lysates, medium, and supernatants and pellets after UV inactivation and ultracentrifugation (see Materials and Methods).

viral particles with a VEEV envelope, was used for infection of a variety of cell lines, including HEK293T, BHK-21, NIH 3T3, and A549/ACE2 cells. The infected cells were incubated in serum-free media. Samples were harvested at 18 hours p.i. and analyzed by WB (Fig. 10). Expression of the S protein by VEErep/S resulted in efficient secretion of S1 into the media from all cell lines used in this experiment (Fig. 10). Based on SDS-PAGE mobility, the S1 proteins secreted from Vero E6, HEK293T, and NIH 3T3 were of the same size. The S1 subunit released from BHK-21 cells appeared to be larger, while the protein produced by A549/ACE2 cells was noticeably smaller. These differences in mobility were likely the results of different glycosylation patterns of the S1 rather than changes in proteolytic processing. Thus, the secretion of S1 was not specific to Vero cells and was largely independent of multiple processes involved in SARS-CoV-2 replication.

S1 subunit is secreted by multiple expression cassettes. Next, we intended to determine whether synthesis of the entire S protein is a prerequisite of the S1 secretion. We cloned sequences of (i) S1 subunit, (ii) S protein without the cytoplasmic peptide, (iii) S protein having no cytoplasmic peptide and transmembrane domain, and (iv) S protein with heterologous trimerization peptide (T4 fibritin foldon) instead of the transmembrane domain under the control of the subgenomic promoters (VEErep/S1, VEErep/SΔCyt and VEErep/SΔTm, and VEErep/Secto, respectively) (Fig. 11A). These

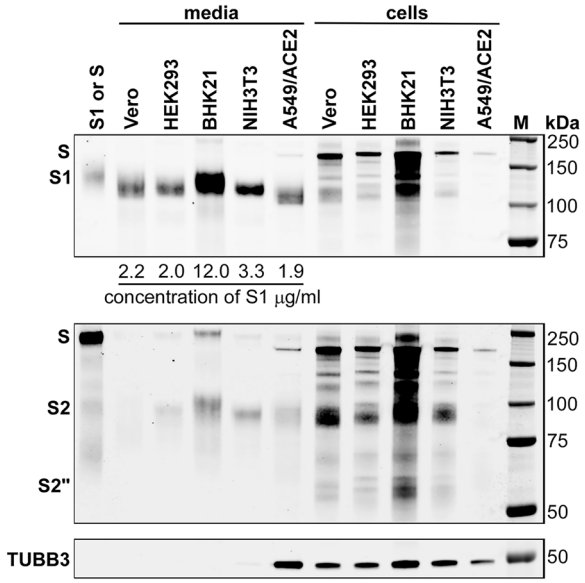

FIG 10 Secretion of S1 subunit after infection with packaged VEErep/S is not cell-specific. The indicated cell lines were infected with VEErep/S, packaged into infectious VEEV particles, at an MOI of 10 inf.u/cell. Infected cells were incubated in serum-free medium for 18 h. The levels of S, S1, and S2 were analyzed in the cell lysates and medium by WB.

replicons were also packaged into VEEV structural proteins and used to infect Vero E6 cells. Media were harvested before CPE development, and secreted proteins were analyzed by WB using S1-specific Abs. As we described above, expression of full-length S protein led to secretion of free S1 but not S2, which remained within the cells (Fig. 11B). Expression of SΔCyt protein also led to secretion of similar amounts of S1. The very low levels of S and S2 could be the result of pseudovirus release. Expression of Secto resulted in secretion of all three forms of S proteins into the media: the entire S, S1, and S2 subunits. The percentages of S1 and S2 in the S protein-derived protein pools were similar, and neither S1 nor S2 proteins were retained within cells (Fig. 11B). This suggested that Secto could be released as a trimer as previously described (34) and very little, if any, free S1 protein was secreted. Expression of SΔTm also led to the release of equal levels of S1 and S2 subunits, but it remains to be seen whether they are released as monomers or trimers. Interestingly, the S1 subunit expressed by VEErep/S1 was efficiently secreted into the media, but in SDS-PAGE, it always migrated slower than the S1 produced during VEErep/S replication, and its mobility was similar to that of commercially available recombinant S1 (Fig. 11B). Most likely, the changes in mobility were the results of different post-translational modifications. Taken together, these data strongly suggested that the secretion of properly processed S1 is dependent on its expression in the context of the entire S protein.

Secreted S1 subunit induces pro-inflammatory response. To date, published data about the pro-inflammatory functions of soluble S1 remain contradictory. This might be a result of using S1 samples derived from different expression cassettes and expressed in different systems. To obtain additional answers, we determined whether the S1 subunit released from infected cells or cells expressing a full-length S can activate TLR4 receptor. In our initial experiments, we used S1 protein released from Vero cells infected with SARS/D614G or VEErep/SΔCyt. Media harvested form SARS/D514G-infected cells was treated by UV and then concentrated in biosafety level 2 conditions. Media from VEErep/SΔCyt-infected cells did not require UV inactivation, but it was similarly concentrated. As a control, we used concentrated media collected from cells infected with VEErep/GFP. Concentrated media were used to treat HEK-Blue hTLR4 cells, a reporter cell line with a colorimetric response to activation of TLR4 receptor. A robust signal was detected after treatment with medium containing S1 produced by

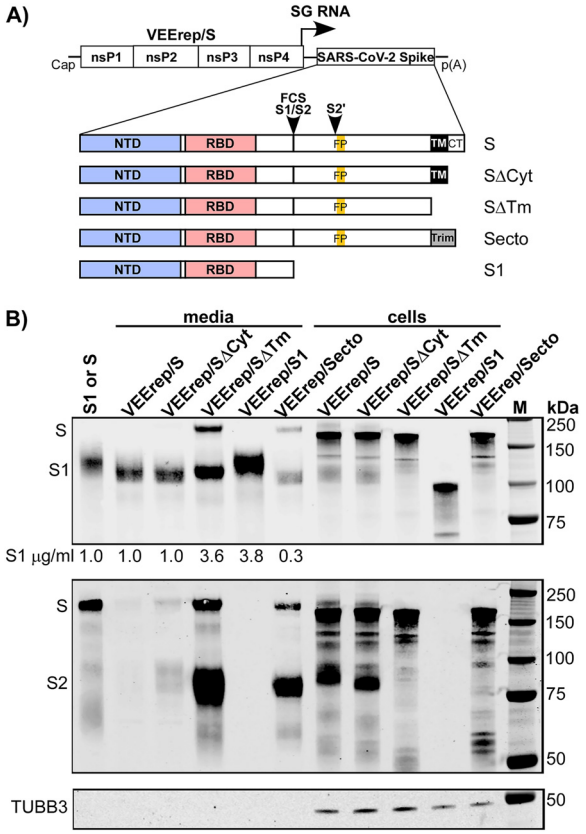

FIG 11 S1, S2, and S proteins can all be expressed in secreted forms. (A) Schematic presentation of the different forms of S protein expressed by VEEV replicons. (B) Vero cells were infected with VEEV replicons encoding different forms of the S protein at an MOI of 10 inf.u/cell. Infected cells were incubated in serum-free medium for 18 h. The levels of S, S1, and S2 were analyzed in the cell-lysates and media by WB. Commercially available recombinant S1 was used for relative quantitation of S1 in different samples.

VEErep/SΔCyt, but not with control medium derived from VEErep/GFP-infected cells (Fig. 12A). This confirmed that secreted S1 activates the TLR4 receptor. However, no signal was detected after treatment with the S1 subunit secreted from SARS/D614G-infected cells. To resolve this ambiguity, we prepared an S1 sample from VEErep/SΔCyt-infected cells, treated it with UV, and concentrated it as performed for the previous viral sample. Next, HEK-Blue hTLR cells were incubated in the presence of the S1 subunit samples, one of which was UV-treated and the second untreated. Without UV treatment, the S1 protein was seen to clearly induce the TLR4-dependent pathway. However, after exposure to UV, it completely lost this activity (data not shown). This provided a plausible explanation for the lack of TLR4 activation by samples of virus-containing media, which were pre-treated with UV light to inactivate infectious virus.

Based on the data, HEK-Blue hTLR4 cells were treated with the S1 subunit-containing media harvested from Vero E6 cells infected with packaged VEErep/S, VEErep/S1, and VEErep/SΔCyt (see Materials and Methods). Identically concentrated medium harvested from cells infected with packaged VEErep/GFP was used as a negative control. In multiple experiments, all of the S1-containing samples reproducibly activated TLR4, albeit those produced by VEErep/S and VEErep/SΔCyt activated TLR4 more efficiently (Fig. 12B). Interestingly, the commercially available S1 did not activate TLR4. This was likely the result of its different post-translational modifications or inactivation during purification and lyophilization procedures utilized during the preparation of this material.

We also tested whether the presence of S1 could lead to activation of pro-inflammatory genes. Within 6 h of S1 treatment, HEK Blue hTLR4 cells clearly demonstrated

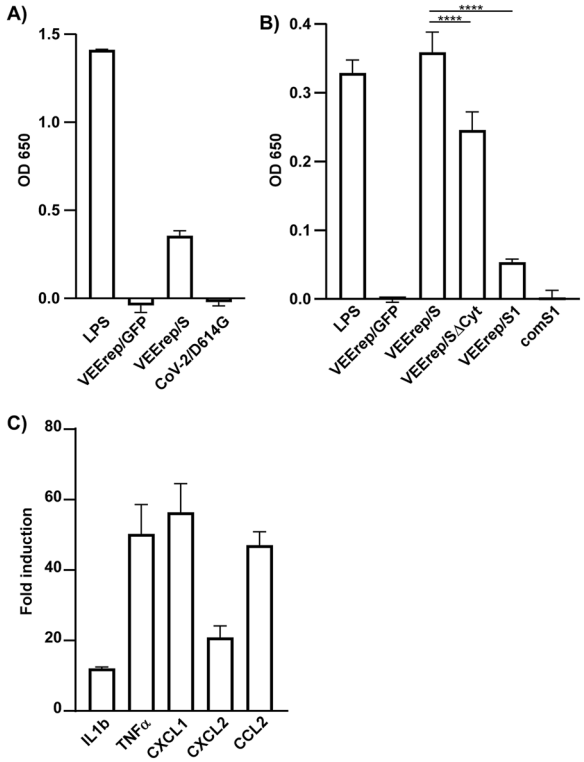

FIG 12 Secreted S1 activates TLR4 receptor. (A) HEK293-Blue TLR4 cells were stimulated by S1 (~1 μg/mL) produced by CoV-2/D614G-infected cells (after inactivation with UV) or by VEErep/S-infected cells (without UV inactivation). Lipopolysaccharide (20 ng/mL) and concentrated media from VEErep/GFP-infected cells were used as positive and negative controls, respectively. Signals were read at 20 h post-stimulation. (B) HEK293-Blue TLR4 cells were stimulated by S1 produced by cells infected with VEEV replicons encoding indicated variants of the S protein. Signals were read at 20 h post-stimulation. Significance of differences was determined by one-way ANOVA Dunnett's test (****, $P < 0.0001$; $n = 3$) (C) HEK293-Blue TLR4 cells were stimulated by S1 (~2.5 μg/mL) produced by VEErep/S-infected cells. The levels of activation of cytokine-specific genes were assessed by qPCR as described in Materials and Methods.

increased concentrations of interleukin-1β-, tumor necrosis factor α (TNF-α)-, CXCL1-, CXCL2-, and CCL2-specific mRNAs (Fig. 12C). This finding provided additional evidence of a pro-inflammatory function of the secreted S1 subunit and suggested the possibility that the released S1 could contribute to pathogenesis in SARS-CoV-2 infections.

DISCUSSION

During the 2-year pandemic, SARS-CoV-2 has demonstrated an unprecedented evolution. One important characteristic of the new variants was that despite using the same ACE2 receptor for cell entry, each new variant appeared to be more transmittable than its predecessors (1–5). Mutations which gradually accumulated in the RBD were found to increase the affinity of the S protein ectodomain to the ACE2 receptor (35), but this effect is unlikely to be the only result of viral evolution. Our data suggest that later isolates have a decreased capacity to infect cells via the catepsins/endosome-mediated entry pathway. In contrast to the earlier circulating CoV-2/WA1 and CoV-2/D614G, the CoV-2/α and CoV-2/δ variants infected Vero/ACE2 cells, which expressed no TMPRSS2, very inefficiently. Compared to that of CoV-2/WA1, the GE:PFU ratio of CoV-2/δ variant determined on Vero/ACE2 cells was more than 4 orders of magnitude higher (Fig. 2A and B). However, the CoV-2/α and CoV-2/δ viruses retained the capacity to infect cells expressing both TMPRSS2 and ACE2. For now, the benefits of shifting to ACE2/TMPRSS2-mediated virus entry for infection spread and pathogenesis remain undefined. Moreover, the GE:PFU ratios of CoV-2/α and CoV-2/δ remain relatively high even on Vero/dKI-high cells that express both TMPRSS2 and ACE2, despite the ability of the viruses to infect these cells (Fig. 2A and C). This effect generally contradicts the

high transmission rates that have been associated with these variants and suggests that *in vivo*, CoV-2/α and CoV-2/δ potentially utilize additional co-receptors or low-affinity binding factors at the plasma membrane. This possibility is supported by earlier findings that SARS-CoV-2 could utilize additional host factors, such as Neuropilin-1 and Integrin, as receptors (15, 16). Interestingly, both CoV-2/α and CoV-2/δ viruses readily returned to the endosome-mediated entry and higher infectious titers in cell culture after acquiring mutations which affected the FCS. This observation raises the additional question of why the S protein of SARS-CoV-2 contains an FCS, which is consistently present in all isolates from patients.

One of the direct consequences of having a fully functional, efficiently processed FCS in the spike protein is that viral replication leads to fusion of ACE2-expressing cells and, even more so, of ACE2/TMPRSS2-expressing cells. Vero/ACE2 cells, which were used in this study, did not exhibit detectable levels of TMPRSS2 yet still supported the formation of relatively small syncytia upon viral infection. This finding was in agreement with previous results which showed that that expression of TMPRSS2 is not an absolute requirement for SARS-CoV-2 induced cell fusion (12). However, the presence of TMPRSS2 greatly increases not only viral infectivity but also the sizes of SARS-CoV-2-induced syncytia. Moreover, overexpression of this serine protease in Vero/dKI-high cells appears to result in the accumulation of aberrantly processed S2 subunits in both S protein-producing cells and viral particles (Fig. 8). These products likely contain S2 in a fusogenic form and further enhance cell-to-cell fusion and viral infectivity.

Syncytium formation may be an alternative mechanism for the spread of SARS-CoV-2 in permissive cells and is believed to contribute to the pathogenesis of SARS-CoV-2 (36–40). The efficiency of cell fusion induced by this virus is particularly evident in CoV-2/δ-infected Vero/dKI cell cultures, in which the entire monolayer rapidly becomes a large syncytium even at a low MOI. Importantly, this mechanism of virus spread is resistant to the presence of high levels of neutralizing hMAbs or Abs from immune sera in the media. In this study, we tested both S1- and S2-specific hMAbs (Fig. 5 and 6D, and data not shown) and two sera with very high neutralizing titers: 7,000 (Fig. 5 and 6D) and 4,000 (data not shown). The antibodies from neither of these preparations could significantly inhibit syncytium formation despite their capacity to completely block infection when mixed with cell-free viral particles. This finding raises the possibility that the induction of Abs capable of interfering with syncytium development could be uncommon. However, a few such Abs have been described in the literature, suggesting that their induction is possible (32, 33). Thus, our data suggest that the presence of FCS in the S protein may make the spread of SARS-CoV-2 infection more resistant to the antiviral effect of virus-specific Abs. This could be of great benefit to allow for more efficient infection, viral transmission, and ultimately circulation in the human population. Unexpectedly, VEEV replicons expressing S protein were found to be capable of forming syncytia in ACE2-expressing cells, particularly in ACE2/TMPRSS2-expressing cells. Moreover, cells infected with this S protein-expressing replicon produced pseudoviruses that could also induce syncytium formation. Thus, this simple replicon-based system could potentially be adapted for screening MAbs that inhibit cell-to-cell fusion and perhaps more importantly, to further define the mechanism(s) of SARS-CoV-2 induced syncytium formation. Currently, the latter aspect of the biology of this virus remains poorly understood.

The second effect of FCS in the S protein was not only the processing of S into S1 and S2 subunits in released virions, but also the efficient secretion of S1 from infected cells. The S1 subunit accumulated in the medium if cells were infected with either SARS-CoV-2 or VEEV replicons expressing the S protein with an intact FCS. The molecular weight of such an S1 and its mobility in the SDS-PAGE gels were different from those of S1 expressed outside the context of the entire S protein (Fig. 11). In addition, the molecular weight also depended on the type of cells used for protein production (Fig. 10). Thus, the post-translational modifications of individually expressed S1 are probably different from those in the trimerized full-length S protein and also cell type-specific.

Although unlikely, it is possible that secreted S1 can decrease the concentration of free neutralizing Abs *in vivo*. However, more importantly, experimental data from this and other studies (41, 42) suggest that free S1 can activate the TLR4 receptor and induce a pro-inflammatory response. A similar effect has previously been described for Ebola virus (43). During replication, this virus also produces large amounts of shed, secreted trimeric glycoprotein GP, which activates a pro-inflammatory response representing a major component of viral pathogenesis (43). This may also be the case for SARS-CoV-2, and questions regarding the benefit of inflammation induction on virus replication and/or spread remain areas of active investigation. Some limited data have suggested a correlation between the concentration of S1 in the plasma and the severity of COVID (44). Importantly, both the Pfizer and Moderna SARS-CoV-2 mRNA vaccines are based on the expression of an S protein with an intact FCS. Thus, after RNA delivery *in vivo*, cells most likely secrete the S1 subunit, which, in turn, can activate a pro-inflammatory response. In fact, it has been demonstrated that, on average, S1 is present in the plasma for 7 days after vaccination (45). Whether its presence plays a positive or negative role in induction of the adaptive immune response and/or adverse reactions associated with these vaccines remains unclear. However, the potential biological activities of S1 should be considered and additionally investigated in future studies.

In conclusion, our study demonstrates that the evolution of SARS-CoV-2 continues during circulation in the human population as evidenced by multiple observations. (i) The most recent variants have become very inefficient in their use of the catepsins/endosome-mediated cell entry pathway and rely more on TMPRSS2-dependent entry. (ii) Acquisition of FCS by the S protein has made SARS-CoV-2 capable of more efficient syncytium formation. The minimal requirement for fusion of infected cells is expression of the ACE2 receptor, but the presence of TMPRSS2 greatly enhances the efficiency of this process. (iii) Overexpression of TMPRSS2 leads to aberrant processing of the S2 subunit. Products of S2 processing accumulate in infected cells and released viral particles. (iv) Cells infected with SARS-CoV-2 or VEErep/S secrete high levels of the S1 subunit. (v) The released S1 is capable of activating the TLR4 pathway and a pro-inflammatory response. This pro-inflammatory function of secreted S1 may be an important contributor to SARS-CoV-2 pathogenesis and to the inflammatory responses to vaccines based on expression of the full-length S protein. In addition, VEErep/S-infected cells release infectious pseudoviruses containing RNA genomes of VEErep/S. These pseudoviruses and VEErep/S represent alternative experimental systems for screening inhibitors of virus entry and syncytium formation.

MATERIALS AND METHODS

Cell cultures. The BHK-21 cells were kindly provided by Paul Olivo (Washington University, St. Louis, MO). Vero E6, NIH 3T3, A549, and HEK293T cells were obtained from the American Type Culture Collection (Manassas, VA). A clone of Vero E6 cells with levels of ACE2 expression undetectable by WB was used in most experiments as an ACE2-negative cell line. Vero/ACE2 cells ectopically expressing hACE2 have been described elsewhere (12). The Vero/dKI-low stable cell line was generated by transfection of Vero/ACE2 cells with PiggyBac plasmid encoding human TMPRSS2, followed by G418 selection. A single clone was selected for further work. Vero/dKI-high cells overexpressing both hAce2 and hTMPRSS2 were obtained from NIAID BEI Resources (no. NR-54970). BHK-21, NIH 3T3, and Vero E6 cells and their derivatives were maintained in alpha minimum essential medium supplemented with 10% fetal bovine serum (FBS) and vitamins. A549, and HEK293T cells were maintained in Dulbecco's modified Eagle medium (DMEM) supplemented with 10% fetal bovine serum.

SARS-CoV-2 isolates. The stock of SARS-CoV-2 strain 2019-nCoV/USA_WA1/2020 (CoV-2/WA1) was derived from one of the first patients diagnosed in the United States. This virus was originally isolated by Natalie Thornburg from the Centers for Disease Control and Prevention in Atlanta, GA (46). It was amplified on Vero E6 cells. Passage 4 was received from the World Reference Center for Emerging Viruses and Arboviruses (WRCEVA) at the University of Texas Medical Branch at Galveston (UTMB). The second early isolate of SARS-CoV-2 (CoV-2/D614G) was described elsewhere (12). It was isolated from a specimen of an unspecified patient on Vero/ACE2 cells, and passage 2 (P2) was used in this study. This virus encoded intact FCS, produced homogeneous small plaques, and demonstrated no heterogeneity in NGS. Other isolates, SARS-CoV2/Alpha and SARS-CoV-2/Delta (termed CoV-2/α and CoV-2/δ, respectively), were recovered on Vero/dKI-high cells from swabs of unspecified patients. These were also represented by homogeneous viral pools. The S proteins of these viruses contained all of the specific

mutations of the B.1.1.7 and B.1.617.2 lineages, respectively. Their stocks were amplified only once. Variants adapted to cell culture were generated by rescuing CoV-2/α and CoV-2/δ on Vero/ACE2 cells. These were termed CoV-2/αAd and CoV-2/δAd, respectively. They had the FCS deleted or mutated, respectively (see Fig. 1B for details).

Viral titers were determined by infecting Vero/ACE2 or Vero/dKI-high cells (2.5×10^5 cells/well) in 6-well Costar plates with serial 10-fold dilutions of the viruses in phosphate-buffered saline (PBS) supplemented with 1% FBS. After incubation at 37°C for 30 min, cells were covered by 0.5% agarose supplemented with DMEM and 3% FBS. After incubation for 3 days at 37°C in a CO_2 incubator, cells were fixed with 7% formaldehyde and stained with 0.5% crystal violet to visualize plaques.

Plasmid constructs. pVEErep/S was designed by cloning the S protein-coding sequence derived from the SARS-CoV-2 (NC_045512.2) genome into Venezuelan equine encephalitis virus TC-83 (VEEV TC-83) replicon under the control of the subgenomic promoter. pVEErep/S1, pVEErep/SΔCyt and pVEErep/ΔTm had the same design but encoded (i) the S1 subunit (amino acids [aa] 1 to 685), (ii) the S protein with a deleted cytoplasmic tail, and (iii) S protein with deleted transmembrane peptide and cytoplasmic tail, respectively. In pVEE/Secto, the C-terminal fragment of S (aa 1,209 to 1273) was replaced with that encoding the T4 fibritin foldon and Flag tag. Plasmids were generated by standard cloning techniques. The plasmids encoding helper RNA of VEEV TC-83 and VEErep/GFP have been described elsewhere (47, 48).

Packaging of VEEV replicons into infectious virions. Plasmids containing cDNAs of VEEV replicons encoding different derivatives of SARS-CoV-2 S protein, and plasmid with helper genome, were purified by ultracentrifugation in CsCl gradients. They were linearized using an MluI restriction site located immediately downstream of the poly(A) tail. RNAs were synthesized *in vitro* by SP6 RNA polymerase in the presence of a cap analog (New England Biolabs) according to the manufacturer's recommendations (New England Biolabs). RNA qualities were assessed by electrophoresis in nondenaturing agarose gels. Replicon and helper RNAs were co-electroporated into BHK-21 cells as described elsewhere (49, 50). Packaged replicons were harvested at 24 h post electroporation. Infectious titers were determined by infecting BHK-21 cells in 6-well Costar plates with serial dilutions of the samples and after incubation at 37°C, cells were fixed with 4% paraformaldehyde (PFA), permeabilized, and stained with S1-specific Abs and fluorescent secondary Abs. Titers were calculated based on the number of S1-positive cells. For replicons encoding wild-type S protein, titers were also determined by infecting Vero/dKI-high or Vero/dKI-low cells with serial dilutions of the samples, incubating at 37°C in complete media for 20 h, fixing with 4% PFA, and staining with 0.5% crystal violet. After this staining, syncytia formed around primarily infected cells were clearly visible.

Virus growth and analysis of the S protein processing and secretion. The subconfluent monolayers of Vero/ACE2 cells were infected with SARS-CoV-2 variants at an MOI of 1 PFU/cell. Cells were then washed 3 times with PBS and further incubated in serum-free VP-SF medium (Invitrogen). To avoid contamination with cell debris and intracellular viral proteins, media were harvested at 16 to 20 hours p.i. before the development of profound CPE. They were passed through 0.22-μm filters and used directly for analysis by WB in most experiments. For some studies, viruses were inactivated by UV treatment for 4 min in a UV Stratalinker 1800, and then 1 mL of virus-containing medium was used to infect Vero/dKI-high cells to confirm lack of infectious virus. Inactivated viruses were pelleted by ultracentrifugation using a TLA-55 rotor in an Optima MAX-TL ultracentrifuge at 54,000 rpm and 4°C for 1 h. Supernatants and pellets were analyzed by WB using S1-, S2-, and N-specific Abs.

Expression of S protein and its derivatives by VEEV replicons. Vero E6 and other cells were infected with packaged VEEV replicons at an MOI of 10 inf.u/cell. They were then washed with PBS and further incubated in VP-SF medium at 37°C in the CO_2 incubator. Media were harvested at 20 hours p.i., at which time cells did not demonstrate any CPE. Collected samples were additionally passed through 0.22-μm filters and used directly for WB. For some experiments, samples were additionally concentrated using Amicon Ultracel-30K Centrifugal filters.

Western blotting. After electrophoresis in NuPAGE 4 to 12% gels (Invitrogen), proteins were transferred to nitrocellulose membranes which were processed with the following antibodies: SARS-CoV-2 S1 (no. 40591-T62, Sino Biological), SARS-CoV-2 S2 (no. 40590-T62, Sino Biological), SARS-CoV-2 nucleoprotein (no. 35-579, ProSci), SARS-CoV-2 nsp1 (no. 10-500, ProSci), GAPDH (glyceraldehyde-3-phosphate dehydrogenase; no. 66004-1-Ig, Proteintech), and β-tubulin (no. 66240-1-Ig, Proteintech). Secondary antibodies labeled with infrared dyes were obtained from Thermo Fisher Scientific: donkey anti-mouse, Alexa Fluor Plus 800 (no. A32789); donkey anti-mouse, Alexa Fluor Plus 680 (no. A32788); and goat anti-rabbit, Alexa Fluor Plus 680 (no. A32734). Membranes were scanned on Odyssey CLX (LI-COR Biosciences) and analyzed in Empiria Studio software (LI-COR).

RNA extraction and RT-qPCR. Total RNA was extracted from a 100-μL viral sample using Direct-zol RNA Miniprep kit (Zymo Research) according to the manufacturer's protocol. cDNA was synthesized using random primers and QuantiTect Reverse transcription kit (Qiagen). qPCRs were performed using a CFX96 Real-Time PCR Detection System (Bio-Rad) in a final volume of 20 μL of SsoFast EvaGreen Supermix (Bio-Rad) supplemented with 500 nM SARS-CoV-2 nsp1-specific forward primer 5′-CCTCAACTTGAACAGCCCTATG-3′ and reverse primer 5′-GAATGCCTTCGAGTTCTGCTAC-3′. The specificities of qPCR products were confirmed by analyzing their melting temperatures. Each PCR was carried out in triplicate. To determine absolute RNA amounts, serial dilutions of SARS-CoV-2 nsp1 standard (2×10^1 to 2×10^7 DNA copies per reaction) were processed in parallel.

Plaque reduction neutralization test. The PRNT was performed as previously described (51). Briefly, serum samples from the unspecified, immunized individuals were incubated at 56°C for 1 h. hMAb 1213H7 (27, 28) and other virus-neutralizing hMAbs were kindly provided by J. Kobie (University

of Alabama at Birmingham). hMAbs and sera were serially (2-fold) diluted in PBS supplemented with 1% FBS and 250 PFU/mL of CoV-2/α. Samples were incubated at 37°C for 1 h, and 0.2-mL aliquots were applied to monolayers of Vero/dKI-high cells in 6-well Costar plates. After a 0.5-h incubation at 37°C, cells were overlaid with 0.5% agarose supplemented with DMEM and 3% FBS. After 3 days of incubation, plaques were stained with crystal violet. The percentage of reduction was plotted against the dilution of sera and concentration of hMAbs to generate slope and intercept values using the best-fit nonlinear curves, which were used to calculate the 50% reduction dilution (GraphPad Prism software).

Inhibition of syncytium formation. In this assay, 6×10^5 Vero/dKI-high cells in 6-well Costar plates were infected with ~100 PFU of CoV-2/α, ~100 inf.u of packaged VEErep/S, or pseudovirus in PBS supplemented with 1% FBS for 1 h at 37°C. Then the inoculums were replaced by 1 mL of DMEM supplemented with 3% FBS and containing hMAbs or immune sera at the concentrations indicated in the figure legends. At 16 to18 hours p.i. (for packaged replicon or pseudovirus) or 2 days p.i. (for CoV-2/α), cells were fixed with 4% PFA and stained for plaques with crystal violet.

Analysis of TLR4 activation by secreted S1 protein. Medium from Vero/dKI-low cells infected by SARS/D614G was collected at 20 hours p.i. and UV-inactivated as described above. The medium was then passed through a 0.22-μm filter, and virion-free samples were generated by ultracentrifugation. Media from cells infected with VEE replicons expressing different S protein variants were passed through a 0.22-μm filter. Supernatants and media were concentrated 20- to 30-fold using Amicon Ultra 30K centrifugal filters (Millipore). The concentrations of S1 subunit were determined indirectly by WB using commercial recombinant S1 with known concentration (no. S1N-C52H3, Acro Biosystems) as a reference. Analysis of TLR4 activation was performed on HEK-Blue hTLR4 cells (no. hkb-htlr4, InvivoGen) according to the manufacturer's instructions (InvivoGen). S1 subunit was added to cells to a final concentration of 1 μg/mL. Lipopolysaccharide from *E. coli* K12 (LPS-EK; no. tlrl-peklps, InvivoGen) was used as a positive control at a concentration of 20 ng/mL. The concentrated samples of VP-SF medium harvested from the cells infected with VEErep/GFP were applied as a negative control.

Stimulation of pro-inflammatory cytokines by SARS-CoV S1 protein. HEK-Blue TLR4 cells were seeded at concentrations of 2×10^5 cells per well in 24-well plates 15 h before stimulation. Samples of secreted S1 protein were prepared as described above in serum-free VP-SF medium harvested from Vero E6 cells infected with packaged VEErep/S replicon. S1 was added to the cells at a concentration of 2.5 μg/mL in DMEM supplemented with 10% FBS. At 6 h post-treatment, cells were collected, and total RNAs were extracted using a Direct-zol RNA MiniPrep kit according to the manufacturer's instructions (Zymo Research). Equal amounts of RNA samples from the S1-treated and mock-treated cells were used for cDNA synthesis by a QuantiTect reverse transcription kit according to the manufacturer's instructions (Qiagen). qPCR was performed using primers specific to *hIL1B* (AAATACCTGTGGCCTTGGGC and TTTGGGATCTACACTCTCCAGCT), *hTNFA* (CCCAGGGACCTCTCTCTAATCA and GCTTGAGGGTTTGCT ACAACATG), *hCXCL1* (AACCGAAGTCATAGCCACAC and CCTCCCTTCTGGTCAGTT), *hCXCL2* (CGCCCAAAC CGAAGTCAT and GATTTGCCATTTTTCAGCATCTTT), *hCCL2* (AGGTGACTGGGGCATTGAT and GCCTCCAGC ATGAAAGTCTC), and 18S rRNA (GAGACTCTGGCATGCTAACTAG and GGACATCTAAGGGCATCAGAG). qPCRs were performed using a CFX Opus 96 real-time PCR detection system (Bio-Rad) in SsoFast EvaGreen Supermix (Bio-Rad). The specificities of qPCR products were confirmed by analyzing their melting temperatures. The data were normalized to the mean threshold cycle (C_T) of 18S rRNA in each sample. The fold differences were calculated using the $\Delta\Delta C_T$ method.

Biohazard. Virus rescue and analyses, which required infectious virus, were performed in the biosafety level 3 (BSL3) facility of Southeastern Biosafety Laboratory (SEBLAB) of the University of Alabama at Birmingham according to the protocols approved by the Institutional Biosafety Committee.

ACKNOWLEDGMENTS

We thank James J. Kobie for providing a panel of neutralizing human monoclonal antibodies.

This study was supported by Public Health Service grants R01AI133159 and R01AI118867 to E.I.F. and R21AI146969 to I.F., and by the UAB Research Acceleration Funds to E.I.F. and I.F.

REFERENCES

1. Mishra S, Mindermann S, Sharma M, Whittaker C, Mellan TA, Wilton T, Klapsa D, Mate R, Fritzsche M, Zambon M, Ahuja J, Howes A, Miscouridou X, Nason GP, Ratmann O, Semenova E, Leech G, Sandkuhler JF, Rogers-Smith C, Vollmer M, Unwin HJT, Gal Y, Chand M, Gandy A, Martin J, Volz E, Ferguson NM, Bhatt S, Brauner JM, Flaxman S, Consortium C-GU. 2021. Changing composition of SARS-CoV-2 lineages and rise of Delta variant in England. EClinicalMedicine 39:101064. https://doi.org/10.1016/j.eclinm.2021.101064.
2. Volz E, Hill V, McCrone JT, Price A, Jorgensen D, O'Toole A, Southgate J, Johnson R, Jackson B, Nascimento FF, Rey SM, Nicholls SM, Colquhoun RM, da Silva Filipe A, Shepherd J, Pascall DJ, Shah R, Jesudason N, Li K, Jarrett R, Pacchiarini N, Bull M, Geidelberg L, Siveroni I, Consortium C-U, Goodfellow I, Loman NJ, Pybus OG, Robertson DL, Thomson EC, Rambaut A, Connor TR, COG-UK Consortium. 2021. Evaluating the effects of SARS-CoV-2 spike mutation D614G on transmissibility and pathogenicity. Cell 184:64–75.e11. https://doi.org/10.1016/j.cell.2020.11.020.
3. Volz E, Mishra S, Chand M, Barrett JC, Johnson R, Geidelberg L, Hinsley WR, Laydon DJ, Dabrera G, O'Toole A, Amato R, Ragonnet-Cronin M, Harrison I, Jackson B, Ariani CV, Boyd O, Loman NJ, McCrone JT, Goncalves S, Jorgensen D, Myers R, Hill V, Jackson DK, Gaythorpe K, Groves N, Sillitoe J, Kwiatkowski DP, Flaxman S, Ratmann O, Bhatt S, Hopkins S, Gandy A, Rambaut A, Ferguson NM, Consortium C-GU. 2021. Assessing transmissibility of SARS-CoV-2 lineage B.1.1.7 in England. Nature 593:266–269. https://doi.org/10.1038/s41586-021-03470-x.
4. Davies NG, Abbott S, Barnard RC, Jarvis CI, Kucharski AJ, Munday JD, Pearson CAB, Russell TW, Tully DC, Washburne AD, Wenseleers T, Gimma

A, Waites W, Wong KLM, van Zandvoort K, Silverman JD, Group CC-W, Consortium C-GU, Diaz-Ordaz K, Keogh R, Eggo RM, Funk S, Jit M, Atkins KE, Edmunds WJ, CMMID COVID-19 Working Group. 2021. Estimated transmissibility and impact of SARS-CoV-2 lineage B.1.1.7 in England. Science 372:eabg3055. https://doi.org/10.1126/science.abg3055.
5. Hou YJ, Chiba S, Halfmann P, Ehre C, Kuroda M, Dinnon KH, 3rd, Leist SR, Schafer A, Nakajima N, Takahashi K, Lee RE, Mascenik TM, Graham R, Edwards CE, Tse LV, Okuda K, Markmann AJ, Bartelt L, de Silva A, Margolis DM, Boucher RC, Randell SH, Suzuki T, Gralinski LE, Kawaoka Y, Baric RS. 2020. SARS-CoV-2 D614G variant exhibits efficient replication *ex vivo* and transmission *in vivo*. Science 370:1464–1468. https://doi.org/10.1126/science.abe8499.
6. Dong E, Du H, Gardner L. 2020. An interactive web-based dashboard to track COVID-19 in real time. Lancet Infect Dis 20:533–534. https://doi.org/10.1016/S1473-3099(20)30120-1.
7. Zhu N, Zhang D, Wang W, Li X, Yang B, Song J, Zhao X, Huang B, Shi W, Lu R, Niu P, Zhan F, Ma X, Wang D, Xu W, Wu G, Gao GF, Tan W, China Novel Coronavirus Investigating and Research Team. 2020. A novel coronavirus from patients with pneumonia in China, 2019. N Engl J Med 382:727–733. https://doi.org/10.1056/NEJMoa2001017.
8. Sola I, Almazan F, Zuniga S, Enjuanes L. 2015. Continuous and discontinuous RNA synthesis in coronaviruses. Annu Rev Virol 2:265–288. https://doi.org/10.1146/annurev-virology-100114-055218.
9. Kung YA, Lee KM, Chiang HJ, Huang SY, Wu CJ, Shih SR. 2022. Molecular virology of SARS-CoV-2 and related coronaviruses. Microbiol Mol Biol Rev 86:e0002621. https://doi.org/10.1128/mmbr.00026-21.
10. Malone B, Urakova N, Snijder EJ, Campbell EA. 2022. Structures and functions of coronavirus replication-transcription complexes and their relevance for SARS-CoV-2 drug design. Nat Rev Mol Cell Biol 23:21–39. https://doi.org/10.1038/s41580-021-00432-z.
11. Xie X, Muruato A, Lokugamage KG, Narayanan K, Zhang X, Zou J, Liu J, Schindewolf C, Bopp NE, Aguilar PV, Plante KS, Weaver SC, Makino S, LeDuc JW, Menachery VD, Shi PY. 2020. An Infectious cDNA Clone of SARS-CoV-2. Cell Host Microbe 27:841–848.e3. https://doi.org/10.1016/j.chom.2020.04.004.
12. Shiliaev N, Lukash T, Palchevska O, Crossman DK, Green TJ, Crowley MR, Frolova EI, Frolov I. 2021. Natural and recombinant SARS-CoV-2 isolates rapidly evolve *in vitro* to higher infectivity through more efficient binding to heparan sulfate and reduced S1/S2 cleavage. J Virol 95:e0135721. https://doi.org/10.1128/JVI.01357-21.
13. Whittaker GR. 2021. SARS-CoV-2 spike and its adaptable furin cleavage site. Lancet Microbe 2:e488–e489. https://doi.org/10.1016/S2666-5247(21)00174-9.
14. Whittaker GR, Daniel S, Millet JK. 2021. Coronavirus entry: how we arrived at SARS-CoV-2. Curr Opin Virol 47:113–120. https://doi.org/10.1016/j.coviro.2021.02.006.
15. Liu J, Lu F, Chen Y, Plow E, Qin J. 2022. Integrin mediates cell entry of the SARS-CoV-2 virus independent of cellular receptor ACE2. J Biol Chem 298:101710. https://doi.org/10.1016/j.jbc.2022.101710.
16. Cantuti-Castelvetri L, Ojha R, Pedro LD, Djannatian M, Franz J, Kuivanen S, van der Meer F, Kallio K, Kaya T, Anastasina M, Smura T, Levanov L, Szirovicza L, Tobi A, Kallio-Kokko H, Osterlund P, Joensuu M, Meunier FA, Butcher SJ, Winkler MS, Mollenhauer B, Helenius A, Gokce O, Teesalu T, Hepojoki J, Vapalahti O, Stadelmann C, Balistreri G, Simons M. 2020. Neuropilin-1 facilitates SARS-CoV-2 cell entry and infectivity. Science 370:856–860. https://doi.org/10.1126/science.abd2985.
17. Leist SR, Dinnon KH, 3rd, Schafer A, Tse LV, Okuda K, Hou YJ, West A, Edwards CE, Sanders W, Fritch EJ, Gully KL, Scobey T, Brown AJ, Sheahan TP, Moorman NJ, Boucher RC, Gralinski LE, Montgomery SA, Baric RS. 2020. A mouse-adapted SARS-CoV-2 induces acute lung injury and mortality in standard laboratory mice. Cell 183:1070–1085.e12. https://doi.org/10.1016/j.cell.2020.09.050.
18. Roy Wong LY, Zheng J, Wilhelmsen K, Li K, Ortiz ME, Schnicker NJ, Pezzulo AA, Szachowicz PJ, Klumpp K, Aswad F, Rebo J, Narumiya S, Murakami M, Meyerholz DK, Fortney K, McCray PB, Perlman S. 2021. Eicosanoid signaling as a therapeutic target in middle-aged mice with severe COVID-19. bioRxiv. https://www.biorxiv.org/content/10.1101/2021.04.20.440676v1.
19. Tang T, Bidon M, Jaimes JA, Whittaker GR, Daniel S. 2020. Coronavirus membrane fusion mechanism offers a potential target for antiviral development. Antiviral Res 178:104792. https://doi.org/10.1016/j.antiviral.2020.104792.
20. Holmes EC, Goldstein SA, Rasmussen AL, Robertson DL, Crits-Christoph A, Wertheim JO, Anthony SJ, Barclay WS, Boni MF, Doherty PC, Farrar J, Geoghegan JL, Jiang X, Leibowitz JL, Neil SJD, Skern T, Weiss SR, Worobey M, Andersen KG, Garry RF, Rambaut A. 2021. The origins of SARS-CoV-2: a critical review. Cell 184:4848–4856. https://doi.org/10.1016/j.cell.2021.08.017.
21. Papa G, Mallery DL, Albecka A, Welch LG, Cattin-Ortola J, Luptak J, Paul D, McMahon HT, Goodfellow IG, Carter A, Munro S, James LC. 2021. Furin cleavage of SARS-CoV-2 spike promotes but is not essential for infection and cell-cell fusion. PLoS Pathog 17:e1009246. https://doi.org/10.1371/journal.ppat.1009246.
22. Hoffmann M, Kleine-Weber H, Pohlmann S. 2020. A multibasic cleavage site in the spike protein of SARS-CoV-2 is essential for infection of human lung cells. Mol Cell 78:779–784.e5. https://doi.org/10.1016/j.molcel.2020.04.022.
23. Lamers MM, Mykytyn AZ, Breugem TI, Wang Y, Wu DC, Riesebosch S, van den Doel PB, Schipper D, Bestebroer T, Wu NC, Haagmans BL. 2021. Human airway cells prevent SARS-CoV-2 multibasic cleavage site cell culture adaptation. Elife 10:e66815. https://doi.org/10.7554/eLife.66815.
24. Klimstra WB, Tilston-Lunel NL, Nambulli S, Boslett J, McMillen CM, Gilliland T, Dunn MD, Sun C, Wheeler SE, Wells A, Hartman AL, McElroy AK, Reed DS, Rennick LJ, Duprex WP. 2020. SARS-CoV-2 growth, furin-cleavage-site adaptation and neutralization using serum from acutely infected hospitalized COVID-19 patients. J Gen Virol 101:1156–1169. https://doi.org/10.1099/jgv.0.001481.
25. Johnson BA, Xie X, Bailey AL, Kalveram B, Lokugamage KG, Muruato A, Zou J, Zhang X, Juelich T, Smith JK, Zhang L, Bopp N, Schindewolf C, Vu M, Vanderheiden A, Winkler ES, Swetnam D, Plante JA, Aguilar P, Plante KS, Popov V, Lee B, Weaver SC, Suthar MS, Routh AL, Ren P, Ku Z, An Z, Debbink K, Diamond MS, Shi PY, Freiberg AN, Menachery VD. 2021. Loss of furin cleavage site attenuates SARS-CoV-2 pathogenesis. Nature 591:293–299. https://doi.org/10.1038/s41586-021-03237-4.
26. Plante JA, Liu Y, Liu J, Xia H, Johnson BA, Lokugamage KG, Zhang X, Muruato AE, Zou J, Fontes-Garfias CR, Mirchandani D, Scharton D, Bilello JP, Ku Z, An Z, Kalveram B, Freiberg AN, Menachery VD, Xie X, Plante KS, Weaver SC, Shi PY. 2021. Spike mutation D614G alters SARS-CoV-2 fitness. Nature 592:116–121. https://doi.org/10.1038/s41586-020-2895-3.
27. Piepenbrink MS, Park JG, Desphande A, Loos A, Ye C, Basu M, Sarkar S, Chauvin D, Woo J, Lovalenti P, Erdmann NB, Goepfert PA, Truong VL, Bowen RA, Walter MR, Martinez-Sobrido L, Kobie JJ. 2022. Potent universal-coronavirus therapeutic activity mediated by direct respiratory administration of a Spike S2 domain-specific human neutralizing monoclonal antibody. bioRxiv. https://www.biorxiv.org/content/10.1101/2022.03.05.483133v1.
28. Piepenbrink MS, Park JG, Oladunni FS, Deshpande A, Basu M, Sarkar S, Loos A, Woo J, Lovalenti P, Sloan D, Ye C, Chiem K, Bates CW, Burch RE, Erdmann NB, Goepfert PA, Truong VL, Walter MR, Martinez-Sobrido L, Kobie JJ. 2021. Therapeutic activity of an inhaled potent SARS-CoV-2 neutralizing human monoclonal antibody in hamsters. Cell Rep Med 2:100218. https://doi.org/10.1016/j.xcrm.2021.100218.
29. Rose NF, Buonocore L, Schell JB, Chattopadhyay A, Bahl K, Liu X, Rose JK. 2014. *In vitro* evolution of high-titer, virus-like vesicles containing a single structural protein. Proc Natl Acad Sci U S A 111:16866–16871. https://doi.org/10.1073/pnas.1414991111.
30. Rose NF, Publicover J, Chattopadhyay A, Rose JK. 2008. Hybrid alphavirus-rhabdovirus propagating replicon particles are versatile and potent vaccine vectors. Proc Natl Acad Sci U S A 105:5839–5843. https://doi.org/10.1073/pnas.0800280105.
31. Zeng C, Evans JP, King T, Zheng YM, Oltz EM, Whelan SPJ, Saif LJ, Peeples ME, Liu SL. 2022. SARS-CoV-2 spreads through cell-to-cell transmission. Proc Natl Acad Sci U S A 119:e2111400119. https://doi.org/10.1073/pnas.2111400119.
32. Asarnow D, Wang B, Lee WH, Hu Y, Huang CW, Faust B, Ng PML, Ngoh EZX, Bohn M, Bulkley D, Pizzorno A, Ary B, Tan HC, Lee CY, Minhat RA, Terrier O, Soh MK, Teo FJ, Yeap YYC, Seah SGK, Chan CEZ, Connelly E, Young NJ, Maurer-Stroh S, Renia L, Hanson BJ, Rosa-Calatrava M, Manglik A, Cheng Y, Craik CS, Wang CI. 2021. Structural insight into SARS-CoV-2 neutralizing antibodies and modulation of syncytia. Cell 184:3192–3204.e16. https://doi.org/10.1016/j.cell.2021.04.033.
33. Tortorici MA, Beltramello M, Lempp FA, Pinto D, Dang HV, Rosen LE, McCallum M, Bowen J, Minola A, Jaconi S, Zatta F, De Marco A, Guarino B, Bianchi S, Lauron EJ, Tucker H, Zhou J, Peter A, Havenar-Daughton C, Wojcechowskyj JA, Case JB, Chen RE, Kaiser H, Montiel-Ruiz M, Meury M, Czudnochowski N, Spreafico R, Dillen J, Ng C, Sprugasci N, Culap K, Benigni F, Abdelnabi R, Foo SC, Schmid MA, Cameroni E, Riva A, Gabrieli A, Galli M, Pizzuto MS, Neyts J, Diamond MS, Virgin HW, Snell G, Corti D, Fink K, Veesler D. 2020. Ultrapotent human antibodies protect against

SARS-CoV-2 challenge via multiple mechanisms. Science 370:950–957. https://doi.org/10.1126/science.abe3354.
34. Cai Y, Zhang J, Xiao T, Peng H, Sterling SM, Walsh RM, Jr, Rawson S, Rits-Volloch S, Chen B. 2020. Distinct conformational states of SARS-CoV-2 spike protein. Science 369:1586–1592. https://doi.org/10.1126/science.abd4251.
35. Rajah MM, Hubert M, Bishop E, Saunders N, Robinot R, Grzelak L, Planas D, Dufloo J, Gellenoncourt S, Bongers A, Zivaljic M, Planchais C, Guivel-Benhassine F, Porrot F, Mouquet H, Chakrabarti LA, Buchrieser J, Schwartz O. 2021. SARS-CoV-2 Alpha, Beta, and Delta variants display enhanced Spike-mediated syncytia formation. EMBO J 40:e108944. https://doi.org/10.15252/embj.2021108944.
36. Braga L, Ali H, Secco I, Chiavacci E, Neves G, Goldhill D, Penn R, Jimenez-Guardeno JM, Ortega-Prieto AM, Bussani R, Cannata A, Rizzari G, Collesi C, Schneider E, Arosio D, Shah AM, Barclay WS, Malim MH, Burrone J, Giacca M. 2021. Drugs that inhibit TMEM16 proteins block SARS-CoV-2 spike-induced syncytia. Nature 594:88–93. https://doi.org/10.1038/s41586-021-03491-6.
37. Rockx B, Kuiken T, Herfst S, Bestebroer T, Lamers MM, Oude Munnink BB, de Meulder D, van Amerongen G, van den Brand J, Okba NMA, Schipper D, van Run P, Leijten L, Sikkema R, Verschoor E, Verstrepen B, Bogers W, Langermans J, Drosten C, Fentener van Vlissingen M, Fouchier R, de Swart R, Koopmans M, Haagmans BL. 2020. Comparative pathogenesis of COVID-19, MERS, and SARS in a nonhuman primate model. Science 368:1012–1015. https://doi.org/10.1126/science.abb7314.
38. Rajah MM, Bernier A, Buchrieser J, Schwartz O. 2022. The mechanism and consequences of SARS-CoV-2 spike-mediated fusion and syncytia formation. J Mol Biol 434:167280. https://doi.org/10.1016/j.jmb.2021.167280.
39. Bussani R, Schneider E, Zentilin L, Collesi C, Ali H, Braga L, Volpe MC, Colliva A, Zanconati F, Berlot G, Silvestri F, Zacchigna S, Giacca M. 2020. Persistence of viral RNA, pneumocyte syncytia and thrombosis are hallmarks of advanced COVID-19 pathology. EBioMedicine 61:103104. https://doi.org/10.1016/j.ebiom.2020.103104.
40. Sanders DW, Jumper CC, Ackerman PJ, Bracha D, Donlic A, Kim H, Kenney D, Castello-Serrano I, Suzuki S, Tamura T, Tavares AH, Saeed M, Holehouse AS, Ploss A, Levental I, Douam F, Padera RF, Levy BD, Brangwynne CP. 2021. SARS-CoV-2 requires cholesterol for viral entry and pathological syncytia formation. Elife 10:e65962. https://doi.org/10.7554/eLife.65962.
41. Shirato K, Kizaki T. 2021. SARS-CoV-2 spike protein S1 subunit induces pro-inflammatory responses via toll-like receptor 4 signaling in murine and human macrophages. Heliyon 7:e06187. https://doi.org/10.1016/j.heliyon.2021.e06187.
42. Olajide OA, Iwuanyanwu VU, Lepiarz-Raba I, Al-Hindawi AA. 2021. Induction of exaggerated cytokine production in human peripheral blood mononuclear cells by a recombinant SARS-CoV-2 spike glycoprotein S1 and its inhibition by dexamethasone. Inflammation 44:1865–1877. https://doi.org/10.1007/s10753-021-01464-5.
43. Escudero-Perez B, Volchkova VA, Dolnik O, Lawrence P, Volchkov VE. 2014. Shed GP of Ebola virus triggers immune activation and increased vascular permeability. PLoS Pathog 10:e1004509. https://doi.org/10.1371/journal.ppat.1004509.
44. Ogata AF, Maley AM, Wu C, Gilboa T, Norman M, Lazarovits R, Mao CP, Newton G, Chang M, Nguyen K, Kamkaew M, Zhu Q, Gibson TE, Ryan ET, Charles RC, Marasco WA, Walt DR. 2020. Ultra-sensitive serial profiling of SARS-CoV-2 antigens and antibodies in plasma to understand disease progression in COVID-19 patients with severe disease. Clin Chem 66:1562–1572. https://doi.org/10.1093/clinchem/hvaa213.
45. Ogata AF, Cheng CA, Desjardins M, Senussi Y, Sherman AC, Powell M, Novack L, Von S, Li X, Baden LR, Walt DR. 2022. Circulating severe acute respiratory syndrome coronavirus 2 (SARS-CoV-2) vaccine antigen detected in the plasma of mRNA-1273 vaccine recipients. Clin Infect Dis 74:715–718. https://doi.org/10.1093/cid/ciab465.
46. Holshue ML, DeBolt C, Lindquist S, Lofy KH, Wiesman J, Bruce H, Spitters C, Ericson K, Wilkerson S, Tural A, Diaz G, Cohn A, Fox L, Patel A, Gerber SI, Kim L, Tong S, Lu X, Lindstrom S, Pallansch MA, Weldon WC, Biggs HM, Uyeki TM, Pillai SK, Washington State 2019-nCoV Case Investigation Team. 2020. First case of 2019 novel coronavirus in the United States. N Engl J Med 382:929–936. https://doi.org/10.1056/NEJMoa2001191.
47. Kim DY, Atasheva S, McAuley AJ, Plante JA, Frolova EI, Beasley DW, Frolov I. 2014. Enhancement of protein expression by alphavirus replicons by designing self-replicating subgenomic RNAs. Proc Natl Acad Sci U S A 111:10708–10713. https://doi.org/10.1073/pnas.1408677111.
48. Gorchakov R, Volkova E, Yun N, Petrakova O, Linde NS, Paessler S, Frolova E, Frolov I. 2007. Comparative analysis of the alphavirus-based vectors expressing Rift Valley fever virus glycoproteins. Virology 366:212–225. https://doi.org/10.1016/j.virol.2007.04.014.
49. Frolov I, Akhrymuk M, Akhrymuk I, Atasheva S, Frolova EI. 2012. Early events in alphavirus replication determine the outcome of infection. J Virol 86:5055–5066. https://doi.org/10.1128/JVI.07223-11.
50. Bredenbeek PJ, Frolov I, Rice CM, Schlesinger S. 1993. Sindbis virus expression vectors: packaging of RNA replicons by using defective helper RNAs. J Virol 67:6439–6446. https://doi.org/10.1128/JVI.67.11.6439-6446.1993.
51. Meshram CD, Lukash T, Phillips AT, Akhrymuk I, Frolova EI, Frolov I. 2019. Lack of nsP2-specific nuclear functions attenuates chikungunya virus replication both *in vitro* and *in vivo*. Virology 534:14–24. https://doi.org/10.1016/j.virol.2019.05.016.